NUMERICAL INVESTIGATION OF SELF-ORGANIZATION AND STABLE BURNING CONDITIONS OF MODERATE PRESSURE GLOW DISCHARGES IN ARGON GAS

A THESIS SUBMITTED TO
THE GRADUATE SCHOOL OF NATURAL AND APPLIED SCIENCES
OF
MIDDLE EAST TECHNICAL UNIVERSITY

BY

ENDER EYLENCEOĞLU

IN PARTIAL FULFILLMENT OF THE REQUIREMENTS
FOR
THE DEGREE OF MASTER OF SCIENCE
IN
PHYSICS

SEPTEMBER 2011

Approval of the thesis:

NUMERICAL INVESTIGATION OF SELF-ORGANIZATION AND STABLE BURNING CONDITIONS OF MODERATE PRESSURE GLOW DISCHARGES IN ARGON GAS

submitted by **ENDER EYLENCEOĞLU** in partial fulfillment of the requirements for the degree of **Master of Science in Physics Department, Middle East Technical University** by,

Prof. Dr. Canan Özgen _____
Dean, Graduate School of **Natural and Applied Sciences**

Prof. Dr. Sinan Bilikmen _____
Head of Department, **Physics**

Assoc. Prof. Dr. İsmail Rafatov _____
Supervisor, **Physics Dept., METU**

Examining Committee Members:

Assoc. Prof. Dr. Serhat Çakır
Physics Dept., METU _____

Assoc. Prof. Dr. İsmail Rafatov
Physics Dept., METU _____

Dr. Ali Alaçakır
Turkish Atomic Energy Institution (TAEK) _____

Assist. Prof. Dr. Hakan Altan
Physics Dept., METU _____

Dr. Burak Yedierler
Physics Dept., METU _____

Date: _____

I hereby declare that all information in this document has been obtained and presented in accordance with academic rules and ethical conduct. I also declare that, as required by these rules and conduct, I have fully cited and referenced all material and results that are not original to this work.

Name, Last Name: ENDER EYLENCEOĞLU

Signature :

ABSTRACT

NUMERICAL INVESTIGATION OF SELF-ORGANIZATION AND STABLE BURNING CONDITIONS OF MODERATE PRESSURE GLOW DISCHARGES IN ARGON GAS

Eylenceoğlu, Ender

M.Sc., Department of Physics

Supervisor : Assoc. Prof. Dr. İsmail Rafatov

September 2011, 50 pages

In this study numerical modelling of a moderate pressure DC glow discharge plasma is carried out in 1D and 2D geometry. The governing equations include continuity equations for the plasma species (electrons, positive ions and metastable atoms), the electron energy equation (EEE), Poisson equation for the electric field in the discharge volume and the surface charge equation on the dielectric side walls. The electron transport coefficients such as the electron diffusion and mobility as well as the electron-impact reaction rates for excitation, ionization and momentum transfer are obtained from look-up tables (LUT). The data in LUTs is tabulated as functions of mean electron energy and obtained from the solution of local Boltzmann equation. Calculations are carried out for the argon gas at 1 and 3 Torr pressures, using COMSOL Multiphysics package. Investigated regimes include subnormal, normal and abnormal glow discharge modes. Current-voltage curves (CVC) and profiles for plasma parameters for the 1 and 3 Torr discharges are developed. Comparison of discharge plasma properties in 1D and 2D, as well as comparison with the available numerical data is performed.

Keywords: glow discharge, modelling, Boltzmann, current-voltage curve, simulation

ÖZ

ORTA BASINÇLI ARGON GAZI IŞILTILI DEŞARJLARININ KENDİLİĞİNDEN YAPILANMASININ VE KARARLI YANMA ŞARTLARININ SAYISAL İNCELENMESİ

Eylenceoğlu, Ender
Yüksek Lisans, Fizik Bölümü
Tez Yöneticisi : Doç. Dr. İsmail Rafatov

Eylül 2011, 50 sayfa

Bu çalışmada orta basınçlı ışıltılı deşarj bir ve iki boyutlu geometride nümerik modellemesi yapılmıştır. Plazma oluşumunu kontrol eden denklem sistemi deşarj bölgesi içinde plazma parçacık çeşitleri için süreklilik denklemlerini (elektronlar, pozitif ionlar ve metastabil atomlar), elektron enerji korunum denklemini (EEE), elektrik alan için Poisson denklemini ve yalıtkan yan duvarlar üstünde yüzey yükü denklemini içermektedir. Uyarma, iyonizasyon ve momentum transferi için elektron çarpışma reaksiyon oranlarıyla birlikte elektron difüzyon ve mobilite gibi elektron transfer katsayıları için yerel Boltzmann eşitliğinin çözülmesiyle ortalama elektron enerjisinin fonksiyonları olarak oluşturulan başvuru tabloları kullanılmıştır. Hesaplamalar 1 Torr ve 3 Torr basınçlı argon gazı için COMSOL Multiphysics paketi kulanılarak yapılmıştır. İncelenen rejimler subnormal, normal ve abnormal ışıltılı deşarj modlarını içermektedir. Sonuç olarak 1 Torr ve 3 Torr basınçlı deşarjlar için akım-voltaj karakteristiği ve deşarj değişkenleri için profiller geliştirilmiş, bir ve iki boyutlu çözümlerde plazma deşarj özellikleri birbirleriyle ve varolan nümerik verilerle karşılaştırılması yapılmıştır.

Anahtar Kelimeler: ışıltılı deşarj, modelleme, Boltzmann, akım-voltaj eğrisi, simülasyon

To my wife...

ACKNOWLEDGMENTS

I would like to thank to Assoc. Prof. Dr. İsmail Rafatov as my supervisor for his contribution with his guidance and patience in the process of completion of this thesis.

I would like to thank to Assoc. Prof. Dr. Serhat Çakır, Dr. Ali Alaçakır, Dr. Burak Yedierler and Assist. Prof. Dr. Hakan Altan for their contributions in the correction process.

I want also to thank to my wife, Zekiye Çıracı Eylenceoğlu, for her patient support and Scientific and Technical Research Council of Turkey (TUBITAK) for financial support during my study.

TABLE OF CONTENTS

ABSTRACT iv

ÖZ v

ACKNOWLEDGMENTS vii

TABLE OF CONTENTS viii

LIST OF TABLES x

LIST OF FIGURES xi

CHAPTERS

1 INTRODUCTION 1

1.1 History 1

1.2 Electric Discharges In Gases 2

1.2.1 Plasma Formation Process 2

1.2.2 Classification and Types of Gas Discharges 3

1.2.3 Parameters of The Gas Discharge Plasma 5

1.3 Processes Occurring In Glow discharges 6

1.3.1 Breakdown Process 6

1.3.2 Collision Processes In The Plasma 9

1.3.3 Processes Occurring At Walls 16

1.4 Structure of Glow Discharges 17

1.4.1 Cathode Layer 18

1.4.2 Negative Glow and Faraday Dark Space 20

1.4.3 Positive Column 21

1.4.4 Anode Layer 21

1.5 Voltage-Current Curve 22

1.6 Basic Modelling Approaches: Classification 23

1.6.1 Kinetic Approach 24
1.6.2 Fluid Approach 24
1.6.3 Hybrid Modelling Approach 25
2 EXTENDED FLUID MODEL OF A DC GLOW DISCHARGE IN ARGON GAS 26
2.1 Aims and Motivation 26
2.2 Two-fluid Plasma Model: Derivation of the Model Equations 27
2.3 Electron Energy Equation 30
2.4 Plasma Transport Coefficients 32
2.5 Plasma-chemical Reactions Taken Into Account 34
2.6 Reaction Rates 35
2.7 Governing Equations 35
2.8 Geometry and Boundary Conditions 37
3 NUMERICAL RESULTS 40
3.1 Numerical Approach 40
3.2 Current-Voltage Characteristics 41
3.3 Comparison of Axial Profiles 42
3.4 2D Profiles 44
3.5 Radial Profiles 45
3.6 Comparison With Different Numerical Data 46
4 CONCLUSION 47
REFERENCES 49

LIST OF TABLES

TABLES

Table 1.1 Discharge types with respect to different frequency ranges [1]. 5

Table 2.1 Collisional reactions that are taken into account in the study [20, 25]. 35

LIST OF FIGURES

FIGURES

Figure 1.1 Discharge tube [1]. 2

Figure 1.2 Various plasma domains in the $n \backsim kT$ diagram [2]. 6

Figure 1.3 The electron avalanche process [11]. 7

Figure 1.4 Paschen curves for different gases [1]. 8

Figure 1.5 Electron collision rate constants for elastic collisions, ionization and excitation in argon gas [2]. 15

Figure 1.6 Layers in a glow discharges with assigned names [1]. 18

Figure 1.7 Distribution of discharge parameters [1]. 19

Figure 1.8 Load line with current-voltage curve for glow discharge [1]. 22

Figure 2.1 Circuit used in the simulations. 27

Figure 2.2 Mobility, μ_e, and diffusion, D_e, coefficients for electrons in $3\,Torr$ pressure argon gas. 34

Figure 2.3 Reaction rate coefficients for (a) direct (K_i) and stepwise (K_{swi}) ionization, (b) excitation-1 (K_{ex1}) and excitation-2 (K_{ex2}), (c) electron impact deexcitation (K_{de-ex}) and (d) elastic collision frequency (ν_{el}) in $3\,Torr$ argon gas tabulated in Table 2.1 36

Figure 2.4 Computational domain used in the study. 38

Figure 3.1 1D and 2D meshes used in the study. 40

Figure 3.2 Voltage-current curves for 1D and 2D simulations for argon gas, $p = 1\,Torr$ and $3\,Torr$, $R = 1.5\,cm$, $L = 1\,cm$. The points are numbered for comparison of axial profiles of plasma parameters in 1D and 2D for subnormal, normal and abnormal regimes. 41

Figure 3.3 Electron (red) and ion (blue) density axial profiles in logarithmic scale, (a) 1D and (b) 2D for subnormal (dotted lines,1), normal (solid lines,4) and abnormal (dash-dot lines,8) regimes in argon discharge, $p = 3\,Torr$. The numbers in parentheses indicate the points in Fig. 3.2-d. The currents corresponding to these points are $I_1 = 9.3\,\mu A$, $I_4 = 3.1\,mA$, $I_8 = 1.6\,A$. 42

Figure 3.4 Comparison of 1D (red) and 2D (blue) calculations for axial electron density (a), ion density (b), potential (c), electric field magnitude (d), electron temperature (e), metastable density (f) profiles for subnormal (dotted lines, 1), normal (solid lines, 4) and abnormal (dash-dot lines, 8) regimes in argon discharge, $p = 3\,Torr$. The numbers in parentheses indicate the points in Fig. 3.2-d. The currents corresponding to these points are $I_1 = 9.3\,\mu A$, $I_4 = 3.1\,mA$, $I_8 = 1.6\,A$. . . 43

Figure 3.5 2D plasma parameter profiles for $p = 3\,Torr$ argon gas, $I = 3.1\,mA$ corresponding to the point 4 labeled in Fig. 3.2-b, $R = 1.5\,cm$ and $L = 1\,cm$. 44

Figure 3.6 Radial current density profiles on cathode surface in logarithmic scale for $p = 3\,Torr$. The numbers indicate the points in Fig. 3.2-b and the corresponding currents for these points are $I_1 = 9.3\,\mu A$, $I_2 = 0.3\,mA$, $I_3 = 1.0\,mA$, $I_4 = 3.1\,mA$, $I_5 = 10.4\,mA$, $I_6 = 30.5\,mA$, $I_8 = 1.6\,A$. 45

Figure 3.7 Comparison of our results (red) with the data in [25] (blue) for 1D calculations where $p = 3\,Torr$ and potential drop between the electrodes, $V_a = 300\,V$. (a) Current-voltage curves, (b) electron and ion density profiles, (c) potential profiles and (d) electron temperature 46

CHAPTER 1

INTRODUCTION

1.1 History

Discharge phenomenon in gases is a well-known natural occurrence almost from the beginning of mankind. Most known and freaky types of this phenomenon are lightning and polar lights (Aurora Borealis) that takes interest of human. First investigations in this area started at the end of eighteenth century by Charles Augustin de Coulomb on the leaking of charge through the air in experimental studies.Through the eighteenth century many contributions to this area were made by different scientists throughout the world. V.V. Petrov's discovery of arc discharge in 1803 and Faraday's studies on glow discharge are the cornerstones in this century. The discovery of electron as a result of J.J. Thomson's works and improvement of atomic physics theory at the beginning of nineteenth century provided a more deeply understanding of discharge mechanisms as ionization and excitation of atoms that is related to the electron flow in gas. Lastly J.S.E. Townsend and Irving Langmuir performed experimental studies based on the measurement of discharge characteristics like current, voltage and electric field etc. founding the basics of discharge physics theory in the modern meaning that all other studies is based on. Since 1930s these studies expanded into various areas such as radio science for communication, controlled nuclear fusion, lighting or display technologies that all of which are related to our daily life [1, 4, 7].

Additionally at the mid-sixties of the twentieth century parallel to the improvement of computers,the first numerical simulations were done by physicists and characteristics of discharge were investigated by realistic models within numerical approaches. Different types of glow to optical discharges were studied by physicists during the last fifty years by making numerical

simulations on computers and the efficiency of these simulations increased with the improvement of processor speeds [11].

1.2 Electric Discharges In Gases

Electric discharges in gases is a term that refers to the flow of charges through a gap between electrodes full of a nonconducting atomic or molecular gas or mix of them, parallel to the breakdown of gas under the condition of sufficiently high voltage between electrodes. The result is a ionized gas which is called "plasma" as fourth state of matter that is formed by charged (electrons, ions) and neutral (metastable, gas atoms or molecules) particles. In fact it is not required a closed circuit or electrodes for all discharge types as in the case of oscillating electric fields, i.e microwave or radio-frequency discharges. In this case basic mechanisms like breakdown, maintaining the ionized state do not differ from the dc discharge in principle but the description of dissipation of energy of the field is made by absorption of radiation instead of release of Joule heat by electric current as in the dc case [1].

1.2.1 Plasma Formation Process

The most known experimental setup that introduces fundamental types of dc discharges is the two metal electrodes inserted into a glass tube and connected to a dc power supply [Fig. 1.1]. An external resistance can be put into the circuit to control the current value. Tube sizes can change from $1\,cm$ to $50\,cm$ as length and $1\,cm$ to $5\,cm$ as radius for experimental purposes. Different types of gas can be filled into the discharge volume at pressures from $1\,Torr$ to $1\,atm$. The voltage between the electrodes and current in the circuit are measured to investigate relation between them [1].

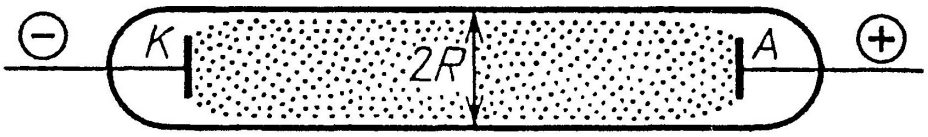

Figure 1.1: Discharge tube [1].

An explanatory description of discharge phenomena in this experiment can be made by in-

creasing voltage between electrodes step by step. At the beginning for low voltages of several tens of volts , there is no apparent effect that can be measured except that a high precision instrument would measure a current on the order of $10^{-15}\,A$ which results from the movement of charges under the effect of the applied electric field that is generated by cosmic rays and natural radioactivity which can ionize the gas at very low levels. Similarly a radioactive or X-ray source can produce a current at $10^{-6}\,A$ level. Still this is not sufficient for the gas to emit light. Up until now we have looked into the non-self-sustaining discharges which actually cannot survive without an external ionizing source or artificial emission of charged particles from electrodes that is front running the neutralization of charged particles on the walls and in the volume . So the current growth and saturation that occur is related to a limited rate of ionization. For a self-sustaining discharge it is required that a self-ionizing source supplies charges to maintain a steady current. For higher voltage values of several hundred volts , at pressure $p \backsimeq 1\,Torr$ and gap length $L \backsimeq 1\,cm$ the electrons that gain energy from the applied electric field or secondary electrons emitted from the cathode under the bombardment of heavy ions and neutrals fulfill this duty, breakdown occurs , the current increases sharply and discharge becomes self-sustaining. This is related to the sufficient energy gained by electrons and ions from the field to ionize neutral particles and make the cathode emit secondary electrons. Process starts with a few electrons moving in the field , the electrons that have gained energy sufficient for ionization energy ionize the gas atoms, electrons proliferate by this way and an electron avalanche occurs in about 10^{-7} to $10^{-3}\,s$. At the result the gas is ionized balanced with charges lost at surfaces and recombination of electrons and ions, furthermore the gas begins to glow if the ionization fraction is sufficiently high [1, 12].

1.2.2 Classification and Types of Gas Discharges

There are several ways of classifying discharges based on the some defined physical features. Mainly the discharges can be described under two main titles as non-self-sustaining discharges which we mentioned above and self -sustaining ones which are more diversified and actually a much larger investigation area for the researchers. Other classification methods are based on more distinctive features like dc or ac for power source used, low or high for pressure, weakly,partially or strongly ionized for ionization degree, thermal or non-thermal for temperature, equilibrium or non-equilibrium for temperature difference between electrons and ions and different frequency range discharges for the electric field. Steady and quasi-

steady self-sustaining discharges include glow discharge, arc discharge, Townsend's dark discharge, corona discharge and spark discharge in a prioritized list.

Glow discharges, which are the most frequently investigated, develop under the conditions of low pressure $1 - 10\,Torr$ and high external resistor to prevent high currents in the circuit. As a result a current of order 10^{-6} to $10^{-1}\,A$ for a tube radius $R \backsimeq 1\,cm$ flows on the discharge volume under a voltage difference of several hundred volts between electrodes. In glow discharges ionization degree is very low on the order of $10^{-8} \backsimeq 10^{-6}$ which are the values for fraction of ionized atoms in gas and the medium can be thought of as electrically neutral (quasineutrality) which is closely related to the concept of "plasma" except for the regions close to the electrodes. Glow discharges are in a non-equilibrium state in respect to the huge temperature difference between the electrons ($T_e \backsimeq 1eV \backsimeq 10^4\,K$) and heavy particles like ions or neutral gas atoms ($T \backsimeq 300 \backsimeq 350\,K$) and are sustained by the low rate of Joule heat release under the conditions of high specific heat of gas and high rate of cooling of gas. This type is studied generally under four subgroups as (1) Townsend's' dark discharge, (2) subnormal, (3) normal and (4)abnormal glow discharges. The last feature that we should mention is the secondary electron emission from a cold cathode under the bombardment of ions. One of the most known example is the glowing tubes used for street advertisements [1, 2].

Arc discharges develop under the conditions of high pressures on the order of atmospheric level and low external resistance to permit high currents after the breakdown of the gas. Relatively high current on the order of $1\,A$ and low potential difference on the order of several tens of volts characterize the voltage-current values of arc discharge. It can be put into the group of equilibrium plasmas with close temperatures of light (electrons) and heavy (ions, atoms) particles as $T_e \backsimeq T \backsimeq 10^4\,K$ and corresponding ionization degree on the order of $10^{-3} - 10^{-1}$. The distinctive feature of arc discharges from glow discharges is related to the mechanism of electron emission from cathode which is a result of heating of the cathode by high current so electrons are emitted by cathode thermionically [1, 8].

First one of the other remaining types is the spark discharge that develops under the conditions of atmospheric pressure and inter-electrode gap $L > 10\,cm$ which ignites by rapid growth of a discharge channel as a short circuit between electrodes with a high ionization degree. Most known example is lighting which uses the clouds and the ground as electrodes. The second one, corona discharge, develops at the existence of strongly nonuniform fields which are

insufficient for the breakdown of the medium at sharp ends of wires with sufficiently high voltage and around power transmission line conductors [1].

Basic features like breakdown in oscillating field discharges, where electrodes are not required, do not differ from a dc field discharge fundamentally. So another classification can be made which does not refer to the electrode effects, based on two properties as state of ionized gas and frequency range of the field. The first one divides discharges into the groups according to breakdown and equilibrium state as (1) breakdown, (2) sustaining non-equilibrium plasma and (3) sustaining equilibrium plasma. The discharges classified according to frequency of the sustaining field refer to the well-known ranges as (1) dc, low-frequency and pulsed fields except for the very short ones, (2) radio frequency, (3) microwave and (4) optical (infrared to ultraviolet) discharges. The intersection of these two main classifications is described in Table-1.1 clearly [1].

Table 1.1: Discharge types with respect to different frequency ranges [1].

	Breakdown	Non-equilibrium plasma	Equilibrium plasma
Constant electric field	Initiation of glow discharges in tubes	Positive column of glow discharge	Positive column of high pressure arc
Radio frequency	Initiation of rf discharges in vessels filled with rarefied gases	Capacitively coupled rf discharges in rarefied gases	Inductively coupled plasma torch
Microwave range	Breakdown in waveguides and resonators	Microwave discharges in rarefied gases	Microwave plasmatron
Optical range	Gas breakdown by laser radiation	Final Stages of optical breakdown	Continuous optical discharge

1.2.3 Parameters of The Gas Discharge Plasma

There are many defined parameters and concepts that characterize plasmas like Debye radius (Debye shield), Larmor radius, plasma frequency, plasma parameter, cyclotron frequency and thermal velocity etc. The three of them, namely, particle density n in m^{-3}, temperature T in eV and (3) steady state magnetic field B in T are the most fundamental ones that all of the above parameters we mentioned can be formulated from. Additionally a classification of plasmas in a wide range of different types can be made using particle density and temperature of electrons which is illustrated in Fig. 1.2 [2].

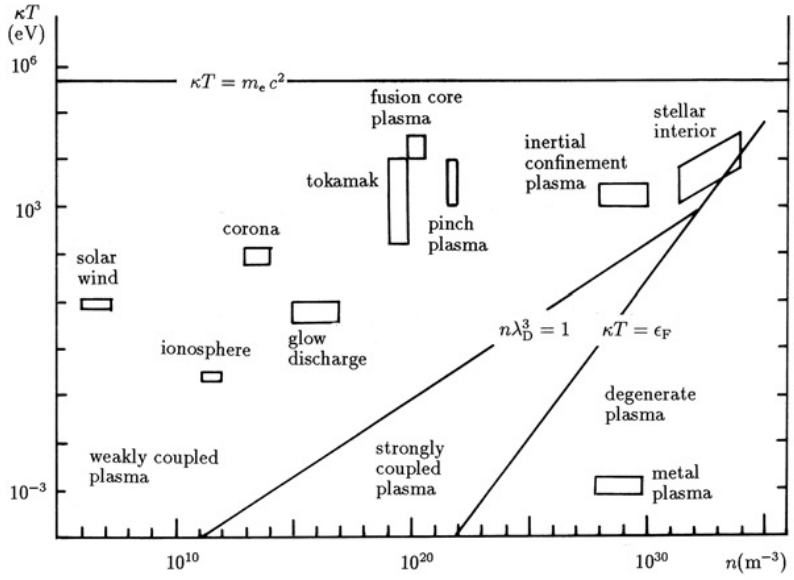

Figure 1.2: Various plasma domains in the $n \backsim kT$ diagram [2].

1.3 Processes Occurring In Glow discharges

1.3.1 Breakdown Process

The breakdown process in discharges refers to the transition from a non-self-sustaining discharge to a self-sustaining one most generally. In the case of glow discharges the well-known "Townsend mechanism" puts a clear explanation for the breakdown of gas based on the phenomena "electron avalanche" that defines the multiplication of a few initial electrons under effect of sufficiently strong electric field applied artificially. The initial electrons could be created by any kind of source like cosmic rays, natural radioactivity or photoelectrons that is emitted from cathode irradiated by a ultraviolet light. At the beginning while the electric field is not very strong a non-self-sustaining discharge is maintained with a steady current I as a result of removal of artificially created charge carriers (electrons, ions) to the electrodes in a balance with out sources. The current reaches a "saturation" value when all of these charges could be removed to the electrodes ignoring electron and ion losses by diffusion and recombination. At this stage the current does not change as the thee voltage increases [1, 2].

When the energy of electrons that is gained under the effect of electric field is sufficient to ionize gas atoms electron impact ionization process starts. In this manner the breakdown process of gases has a threshold value for the voltage between electrodes or electric field

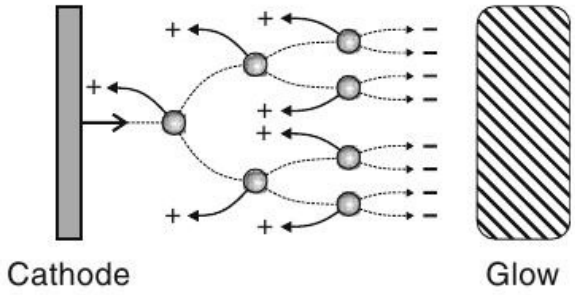

Figure 1.3: The electron avalanche process [11].

in the medium. The initial electrons accelerated by the field ionize the gas atoms creating additional electron and ion pairs. New electrons goes on the same way and they create pairs by ionization too. So the phenomena "electron avalanche" occurs on the way between cathode and anode [Fig-1.3]. This process was first formulated by Townsend as expressing the number of electrons increasing exponentially from cathode to anode [1, 2],

$$dN = N\alpha(x)dx, \tag{1.1}$$

where α is the Townsend coefficient that describes the number of electron-ion pairs created per unit length by one electron and N is electron number density. This coefficient depends on the ionization frequency ν_i via the drift velocity v_d as

$$\alpha = \frac{\nu_i}{v_d} \tag{1.2}$$

that depends on the reduced electric field E/p, where p is pressure, and the gas type that exists in the discharge volume. Integrating this equation gives an equation for the number of electrons as

$$N(x) = N_0 exp(\int_0^x \alpha(x')dx') \tag{1.3}$$

where N_0 is the number of electrons at cathode. Additionally ions created on this way are moved to the cathode by the electric field and this bombardment of ions causes a secondary electron emission process in this region which contribute to the multiplication of electrons effectively. This secondary contribution is expressed by a coefficient γ, which is the number of electrons emitted from the cathode surface for every ion. The number of ions created on the way from cathode to the anode that arrives at the cathode by ignoring losses is [1, 2]

$$N_i = N_0[exp(\int_0^d \alpha(x')dx') - 1] \tag{1.4}$$

where d is electrode separation distance. The number of electrons emitted from cathode corresponding to this value which can be accepted as equal to N_0,

$$N_{se} = N_0 = \gamma N_0[exp(\int_0^d \alpha(x')dx') - 1], \tag{1.5}$$

that results in a condition for breakdown of the gas as

$$exp(\int_0^d \alpha(x')dx') = 1 + \frac{1}{\gamma}. \tag{1.6}$$

The expression above provides us a clear explanation for the threshold behavior of breakdown process where the right-hand is constant but left-hand side changes dependent on the value of α. Generally the spatial dependence of this value is expressed via reduced electric field E/p experimentally as

$$\alpha = Apexp(-\frac{B}{E/p}) \tag{1.7}$$

where A and B are the constants depending on the gas type. Shortly after the breakdown electric field is not distorted considerably and this coefficient can be accepted as constant that putting it in (1.6) gives the solutions for reduced electric field and voltage for breakdown [2],

$$\frac{E}{p} = \frac{B}{ln[\frac{Apd}{ln(1+1/\gamma)}]}, \qquad V_b = \frac{Bpd}{ln[\frac{Apd}{ln(1+1/\gamma)}]}. \tag{1.8}$$

The breakdown voltages for different gases is plotted in Fig. 1.4 named as Paschen curves.

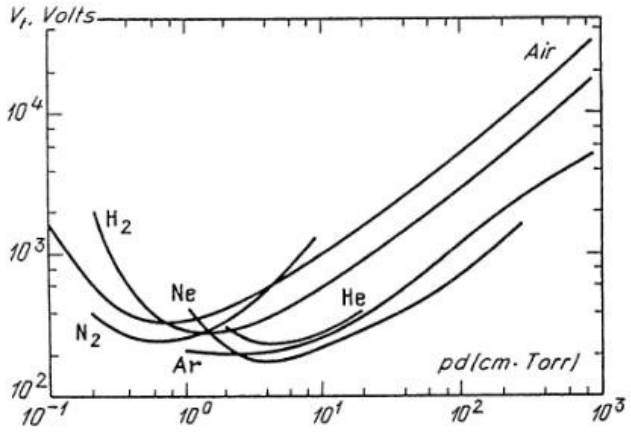

Figure 1.4: Paschen curves for different gases [1].

1.3.2 Collision Processes In The Plasma

Basics

Collision processes in a discharged gas determine the main characteristics of the plasma in a direct way. First-hand obvious result is the spatial diffusion of particles in the volume. Additionally some properties of colliding particles like mean energy, mobility or the ionization degree of a plasma can be affected by the collision processes between these particles. From most general point of view the collisions can be grouped into two types as elastic and inelastic ones. In elastic collisions momentum and kinetic energy is conserved in the mean that only exchange of these variables is possible. Coulomb scattering between charged particles and polarization scattering between a charged and a neutral particle is included in this group. The inelastic collisions, where kinetic energy is not conserved,is directly related to the discharge phenomena, include ionization, excitation and recombination mainly together with deexcitaion, association or attachment for electronegative gases. The rate of the collisions between charged particles (electron-ion, electron-electron, ion-ion) or charged particles and neutral gas atoms (electron-neutral, ion-neutral) are related to the ionization degree in the discharge volume. The classification of plasmas based on this parameter as weakly, partially or strongly ionized refers to which type of collisions is dominant in the volume, charged-charged or charged-neutral [2].

The basic parameter that characterize collisions is cross-section $\sigma(v)$, which can be described as effective interaction area for particles during collisions. It depends on the nature of the force as short-ranged (hard sphere collisions) or long-ranged (Coulomb interaction) between the particles and relative velocities .All other quantities like mean free path, collision frequency or rate constant can be formulated by using $\sigma(v)$ in simple manner below.

For incoming particles with density n and heavy target particles with density N, let us consider the cross-section $\sigma(v)$ be independent of the relative velocity v (hard sphere). The number of total collisions in which an incoming particle is removed from its usual orbit by this way can be written for a volume of thickness dx [2],

$$dn = -n[N[\sigma dx]] = -\sigma n N dx. \tag{1.9}$$

Solving this equation gives us the change in the number of incident particles in an exponential

form,

$$n(x) = n_0 exp(-x/\lambda), \tag{1.10}$$

where λ is mean free path defined as

$$\lambda = \frac{1}{\sigma N}, \tag{1.11}$$

which describes the distance for decrease of the uncollided incoming particle number density to $1/e$ of its initial value n_0. Using the velocity v of the incoming beam the mean time between collisions is formulated as

$$\tau = \frac{\lambda}{v} = \frac{1}{\sigma N v}. \tag{1.12}$$

Inverse of this quantity defines the frequency for collisions that is the number collisions per second,

$$\nu = N\sigma v. \tag{1.13}$$

If we define collision frequency per unit density of heavy particles we get the rate constant

$$K = \frac{\nu}{N} = \sigma v. \tag{1.14}$$

The dependence of cross-section on velocity is expressed by using differential cross-section that is defined as the number of particles leaving the interaction volume through the differential part of the total one. It is formulated by using a impact parameter b and the angle θ for the differential part related to the velocity

$$I(v, \theta) = \frac{b}{sin\theta} \left| \frac{db}{d\theta} \right|. \tag{1.15}$$

Integrating this gives the total cross-section

$$\sigma(v) = 2\pi \int_0^\pi I(v, \theta) sin\theta d\theta. \tag{1.16}$$

In most calculations the momentum cross-section is more useful than the above that is directly related frictional force due to collisions and is defined as

$$\sigma_m(v) = 2\pi \int_0^\pi (1 - cos\theta) I(v, \theta) sin\theta d\theta. \tag{1.17}$$

Elastic Collisions

Elastic collisions can be important for energy transfer in collisions between particles that have comparable masses. The fraction of energy loss for an incoming particle is proportional to

$\delta = 2M_R/M_{rest}$ where M_R is reduced mass. In the case of electron-ion or electron-neutral elastic collisions this leads to a little energy transfer fraction on the order of 10^{-4} so results in very distinct temperatures as $T_e >> T_g$, where T_e is electron temperature and T_g is gas temperature. For the case of ion-neutral collisions, $\delta = 1/2$ which forces them to be of the same temperature as $T_i = T_g$, where T_i is ion temperature.

Coulomb scattering between charged particles and polarization scattering of a charged particle in an interaction with a neutral particle are two dominant types that can be included in this group. The former occurs due to the long-ranged Coulomb force so it has large cross section value for a collision. In this manner Coulomb scattering can be an effective collision process in a discharged gas with a ionization degree on the order of one percent or higher. The calculation of total cross -section for Coulomb scattering by using differential cross-section definition leads to an infinite value as a result of long-range character of Coulomb force. The solution to this problem can be found by using the effect of Debye shielding by assigning maximum impact parameter value as the Debye radius, $b_{max} = \lambda_{De}$, that results in a effective cross section. Scatterings through small angles do not affect discharge properties effectively, so cross-sections for large angle scatterings, which occur in two ways as a single scattering with a large angle and a large angle scattering as a result of accumulation of small angle scatterings, can be more useful for quantitative aims. The calculated formulas for these types are [2]

$$\sigma(simple) = \frac{1}{4}\pi b_0^2, \qquad \sigma(cumulative) = \frac{8}{pi} b_0^2 ln\Lambda \tag{1.18}$$

where b_0 is the classical distance of minimum approach and $\Lambda = 2\lambda_{De}/b_0$. Comparison of these two values shows us that the lateral, cumulative large angle scatterings, is dominant on the former by a factor of several tens. Lastly it is important to mention strong dependence of of Coulomb cross-section on velocity via b_0,

$$\sigma \backsim b_0^2 \backsim \frac{1}{v^2}, \tag{1.19}$$

where this shows that low velocity particles are scattered more effectively [2].

The lateral, polarization scattering, which is the main collisional process in a weakly ionized plasma, comes true by the interaction of a charged particle with the short-ranged field of a neutral particle that is polarized by the incoming charged particle itself. This type of interaction is possible for ions and only for low energy electrons because a neutral gas atom does not have sufficient time to polarize with an energetic electron. The characterizing parameter

that is known as Langavin or capture impact parameter b_L divides polarization scatterings into two groups as hyperbolic orbits for $b > b_L$ and capture orbits which spirals into the atom for $b < b_L$ that results in a large scattering angle by reflection from the core of the atom or an inelastic collision by interaction of two particles strongly. The capture cross-section is formulated as

$$\sigma_L = \pi b_L^2 = \left(\frac{\pi \alpha_p q^2}{\varepsilon_0 M}\right)^{\frac{1}{2}} \frac{1}{v} \tag{1.20}$$

that leads to capture rate constants for electrons and ions,

$$K_{Le} = 3.85 \cdot 10^{-8} \alpha_R^{1/2} cm^3/s, \qquad K_{Li} = 8.99 \cdot 10^{-10} \left(\frac{\alpha_R}{A_R}\right)^{1/2} cm^3/s, \tag{1.21}$$

where α_p is polarizability, α_R is the relative polarizability, v is relative velocity, A_R is reduced mass, M is rest gas atom mass and q is charge of incoming charged particle [2].

Ionization

Ionization is the most important mechanism in discharge volume to maintain a self-sustaining state, especially the electron impact ionization. This process is characterized by ionization frequency ν_i or by a dependent quantity as reaction rate constant κ_i, which is the ionization frequency for unit density of gas atoms. The frequency has to be averaged over energy distribution function of electrons and is written using the ionization cross-section as

$$\nu_i = n_g < \sigma(v)v >= n_g \int f(\varepsilon)\sigma_i(\varepsilon)v d\varepsilon, \tag{1.22}$$

where ν_i is mean ionization frequency, $\varepsilon = \frac{1}{2}\frac{mv^2}{e}$ and $f(\varepsilon)$ is normalized electron energy distribution function. The electron energy distribution function depends on elastic and inelastic collision processes and can be obtained by solving Boltzmann kinetic equation or experimentally. The temporal change of electron number density can be expressed as [1]

$$dn_{ei} = \nu_i n_e dt = \kappa_i n_g n_e dt. \tag{1.23}$$

The required cross-section formulated classically is

$$\sigma_i(\varepsilon) = \pi \left(\frac{e}{4\pi\varepsilon_0}\right)^2 \frac{1}{\varepsilon}\left(\frac{1}{\varepsilon_{iz}} - \frac{1}{\varepsilon}\right) \tag{1.24}$$

called the Thomson cross-section where ε_{iz} is ionization potential and $\varepsilon > \varepsilon_{iz}$. It has a maximum value at $\varepsilon = 2\varepsilon_{iz}$. A more detailed classical derivation is made by Smirnov [2] taking

care of orbital electron motion and radial distribution resulting in a formulation

$$\sigma_i(\varepsilon) = \frac{\pi}{4}\left(\frac{e}{4\pi\varepsilon_0}\right)^2 \frac{1}{\varepsilon}\left(\frac{5}{3\varepsilon_{iz}} - \frac{2\varepsilon_{iz}}{3\varepsilon^2} - \frac{1}{\varepsilon}\right), \tag{1.25}$$

which has a maximum value at $\varepsilon = 1,85\varepsilon_{iz}$. All of these formulations give a quantitative value on the order of $10^{-16}cm^2$. A quantum mechanical approach leads to a change of the form $\sigma \backsim ln(\varepsilon)/\varepsilon$. Generally the ionization events are caused by high energy tail of electron energy distribution that leads to an electron temperature T_e lower than ionization potential of atoms, $T_e < \varepsilon_{iz}$, on the order of $1 - 2eV$ [2].

The other mechanisms of ionization different from ionization of the gas atoms by direct electron impact can play important roles in weakly ionized gases. First example is stepwise ionization based on two steps as excitation of atoms by electron impact and ionization of these excited atoms by subsequent collisions, where a sufficient time is needed for ionization of these atoms as in long-lived metastable atoms. The order of cross-section for this type is also $10^{-16}cm^2$ [1].

A second example is ionization by excited atoms if excitation energy of incoming atom is larger than the ionization potential of the target atom, $E^* > U_{iz}$. The cross sections for this type of ionization is on the order of $10^{-15}\,cm^2$ for long-lived metastable atoms which is smaller than for the resonance-excited atoms that is on the order of $10^{-14}\,cm^2$. However the density of metastable atoms is greater than resonance-excited ones, because of long lifetime for metastable atoms that leads to a more effective contribution to ionization process with respect to the resonance-excited ones, totally [1].

Thirdly associative ionization based on the association of an excited atom and an neutral gas atom into a molecular ion, $A + A^* \rightarrow A_2^+ + e$, that can contribute to the ionization process in a discharge. This mechanism has a cross-section on the order of $10^{-16} \backsim 10^{-15}\,cm^2$ changing with respect to the type of gas [1].

Lastly, photoionization of atoms has cross-section on the order of $10^{-18} \backsim 10^{-17}\,cm^2$ and can not compete with the electron impact ionization under discharge conditions generally but it can provide initial electrons for electron multiplication process that is based on electron impact ionization.

Excitation and Deexcitation

An atom can undergo an excitation process as well as ionization as a result of electron impact or external radiation from its ground state to higher level energy state. Generally the resulting excited atom tries to return to some lower energy levels or to the ground state by emitting a photon known as electric dipole radiation or deexcitation process,

$$e + A \longrightarrow A^* + e \longrightarrow A + e + \hbar w. \tag{1.26}$$

The characterizing phenomena is the existence of quantum mechanical selection rules that permit or prevent these excitation or deexcitation processes,

$$\Delta l = \pm 1, \qquad \Delta J = 0, \pm 1. \tag{1.27}$$

These selection rules divide excited atoms into two groups as resonance-excited atoms and metastable atoms. The formers deexcite by electric dipole radiation by applying selection rules at short time scales, $10^{-9}\ s$, compared to characteristic collision times for electrons, $\tau_e \backsimeq 10^{-7}\ s$ for $T_e = 3\,eV$ and $p = 10\,mTorr$, and for ions $\tau_i \backsimeq 10^{-5}\ s$ under the same conditions. On the other hand, metastable atoms cannot radiate by electric dipole radiation due to be involved in an excited state which deexcitation is forbidden by selection rules. These atoms can go in other deexcitation processes such as electric quadrupole or radiationless transition to the nearly equal energy states that are not forbidden but these processes are generally weak and have long transition times compared to the collision times τ_e or τ_i, which are on the order of $10^{-3}\ s$. As a result metastable atoms can reach effective densities due to this long life time in the discharge volume [2],

$$\tau_{rad} << \tau_e < \tau_i << \tau_m.$$

A quantum mechanical approach leads to smaller cross-sections for transitions in forbidden states than ones in allowed optical levels by electron impact excitation. The cross-section for excitation can be derived by using a average excitation energy ε_{ex} as in the procedure for ionization cross-section. This leads to the same behavior for energy dependence but shifted to lower energies as a result of $\varepsilon_{ex} < \varepsilon_i$ (Fig. 1.5) [2, 5].

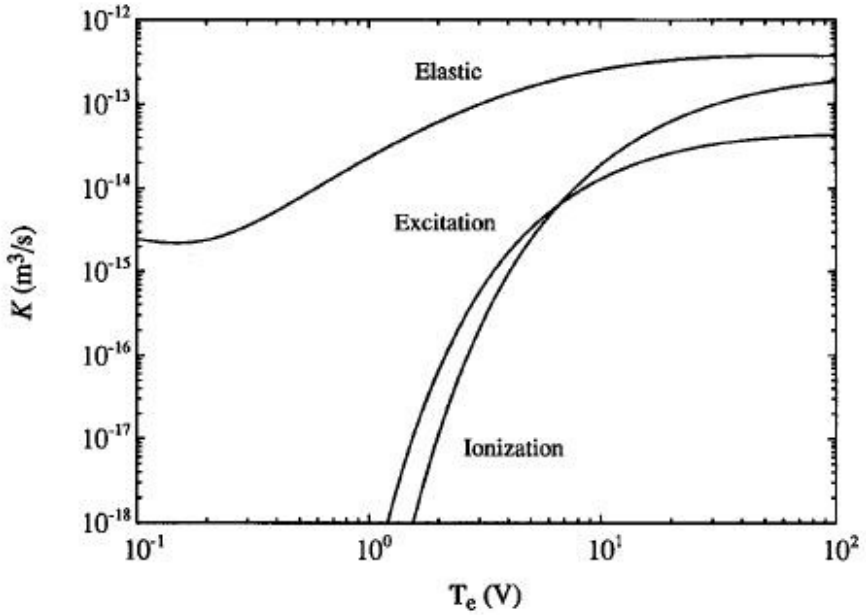

Figure 1.5: Electron collision rate constants for elastic collisions, ionization and excitation in argon gas [2].

Recombination

Charge decay processes are characterized by a recombination coefficient β that corresponds to reaction rate constant in typical discharges which is formulated as

$$dn = -\beta n_e n_i dt.$$

The fastest mechanism for charge decay in the discharge volume is dissociative recombination for weakly ionized plasmas,

$$A_2^+ + e \longrightarrow A + A^*,$$

that has a recombination coefficient on the order of $\beta_{dis} \backsimeq 10^{-7}\, cm^3/s$, which decreases for increasing energy as $T_e^{-1/2}$ and as $T_e^{-3/2}$ for more higher temperatures [1].

A more slow mechanism is the radiative recombination that has a very small collision cross section, $\sigma_r \backsim 10^{-21}\, cm^2$,

$$A^+ + e \longrightarrow A + \hbar w,$$

so that the corresponding recombination coefficient on the order of $10^{-12}\, cm^3/s$ is very small compared to the diffusional loss of charged particles to the walls. The energy dependence of this coefficient is formulated as [1]

$$\beta_{rr} =< \sigma v >= 2.7 \times 10^{-13}\, T_e(eV)^{-3/4}\, cm^3/s.$$

This type of recombination is important as a mechanism of light emission but not effective in recombinational removal of charged particles.

1.3.3 Processes Occurring At Walls

Surface processes can play important roles on the properties of a discharge. Including neutrals arriving at surfaces, it includes many processes such as adsorption, desorption, sputtering, etching or fragmentation in addition to the neutralization of charges on surfaces and secondary electron emission from cathode surface. These processes are described by certain physical and chemical bonds with the surface and characterized by the sticking or flux loss probability coefficients. The well-known secondary electron emission from cathode due to ion bombardment has an effective contribution to maintain a self-sustaining plasma [2].

Neutralization

The surfaces are treated as "black holes" for charged particles (electrons, ions) due to the fact that almost all electron-ion pairs arrive at the surfaces recombine there and re-inject as neutral atoms into the discharge volume. Bulk recombination of electrons and ions in the volume has a very small rate coefficient as we mentioned above that is almost negligible. However on the surfaces a three-body recombination reaction is fast enough to neutralize charges as

$$e + A^+ + S \longrightarrow S + A.$$

If the directed fluxes for electrons and ions to the discharge walls are compared, the difference in fluxes gives a charge accumulation on the walls, which is generally negative due to larger flux of electrons than ions [2].

Secondary Electron Emission

This process is caused by directed motion of several kinds of particles such as positive ions, excited atoms, electrons or photons towards the cold cathode. It is a well-known phenomena that has effective contribution to the breakdown of a discharge gap to maintain a self-sustaining plasma.

Electron emission as a result of positive ion bombardment is the most important one of these secondary mechanisms. It is based on quantum mechanical tunneling of electrons that are confined within a solid wall by a potential barrier of level equal to the work function of solid. Actually the kinetic energies of ions are not sufficient and ineffective for knocking out electrons from the walls. The process is realized by a potential well is being transformed into a potential barrier due to a close positive ion, so this allows an electron to tunnel into the ion to neutralize it. There are two possible ways for this process. First one is tunneling of electron into an excited state which results in a radiative deexcitation into a ground or metastable state. For the second one, electrons tunnel directly into the ground state so that a second electron absorbs the excess energy of neutralization event to escape from the surface. This second mechanism is known commonly as secondary electron emission, but known also as "Auger emission" [1, 2].

This process is characterized by a coefficient γ which is the number of electrons emitted from cold cathode surface per incoming particle. The value of these coefficients changes with respect to the sort of discharged gas, electrode material, incoming particle type or to the impurity of the cathode surface. In the case of ion-electron emission process the value of this coefficient is independent of the ion kinetic energy ε_i up to the $1\,keV$, for instance $\gamma_i = 0.09$ for Ar^+ ions and tungsten electrode. Also metastable atoms of inert gases can yield a secondary electron emission effectively, $\gamma_m = 0.4$ for Ar^* and Cs electrode. The value of this coefficient for electrons, γ_e, varies from 0.4 to 1.6 for different metals with ε_e up to several keVs and $\gamma_\nu \backsimeq 10^{-3} \backsim 10^{-1}$ for the region between visible to ultraviolet light [1].

Secondary electron emission can also occur on dielectric surfaces such as glass and quartz, $\gamma_e \backsimeq 1-3$, which has a maximum value at $\varepsilon_e \backsimeq 300-400\,eV$. In this case incoming electrons are attached to the surface which results in a charge accumulation on the surface, which has negative sign if $\gamma_e < 1$ ($\varepsilon_e < 50\,eV$) or positive sign if $\gamma_e > 1$ [1].

1.4 Structure of Glow Discharges

The structure of glow discharges shows a stratified behavior due to dark and luminous layers developed in the formation process (Fig. 1.6). Each of these layers, which are assigned by a name, are characterized by different properties related to intensity of light emission and

profiles for discharge parameters such as electric potential, electric field, particle densities or fluxes of charged particles (Fig. 1.7). A glow discharge is self-sustaining with effective

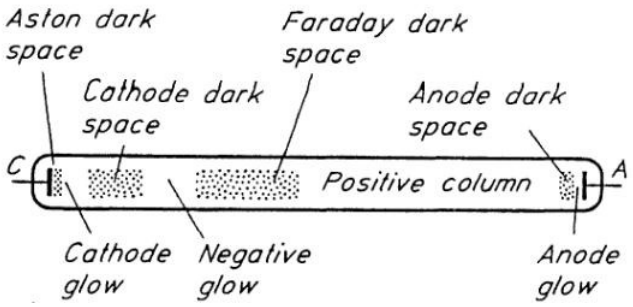

Figure 1.6: Layers in a glow discharges with assigned names [1].

contribution of secondary electron emission from a cold cathode. The feature that separates glow discharges from others is a layer with large positive space charge, a strong electric field and effective potential drop of order $100 - 400\,V$ near the cathode, and actually all these properties are interrelated. This region is called a cathode layer and the considerable decrease in potential is called a "cathode fall". Another characterizing layer is the "positive column" that is not vital as cathode layer and is the most known example of the weakly ionized non-equilibrium plasma in the literature [1].

Depending on some macroscopic parameters such as pressure or electrode separation, all these layers are adjusted with respect to the changes in these variables. For a low pressure, $p \backsim 10^{-2}\,Torr$, and moderate separation of electrodes, positive column formation is prevented and negative glow emission is dominant. For the pressures not too low, it is observed positive column mostly. For high pressures, $p \backsim 100\,Torr$, all layers get thinner and shift towards the cathode. If electrode separation is decreased at constant pressure positive column is shortened although transition layers between column and cathode are not affected. As decreasing of separation is continued, firstly column disappears, then Faraday space goes out, and finally negative glow dies away [1].

1.4.1 Cathode Layer

Cathode layer as a whole is described by a large positive space charge and considerable change in potential with high field strength at the cathode surface. Through the layer, field decreases to very low values before going into the negative glow.

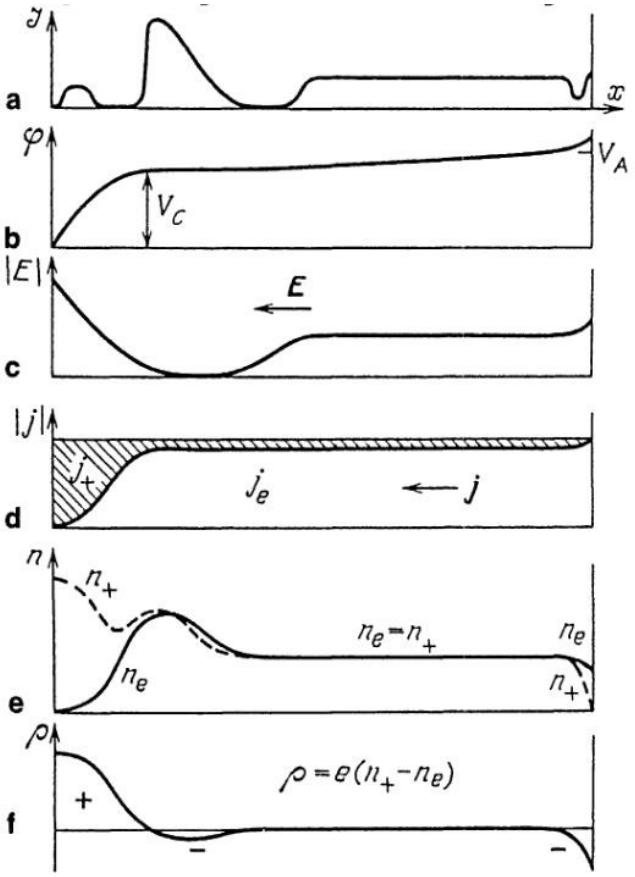

Figure 1.7: Distribution of discharge parameters [1].

The formation of cathode layer is related to the to the efficiency of multiplication of electrons in a strong field under a minimum breakdown voltage, V_{min}. When the current is increased after the breakdown throughout Townsend dark discharge, undisturbed electric field of this region cannot provide this increase via Townsend mechanism due to low electric field. This case results in concentration of the potential fall near the cathode surface by the help of accumulated large positive space charge that causes sufficiently strong electric field. This causes a high ion flux directed onto the cold cathode, which is still incapable of compensating the full current but with the contribution of secondary electron emission as a result of ion flux, the electron density grows exponentially under the strong field by Townsend mechanism in this region and steady current is maintained [1, 3].

The analytical theory of the cathode layer developed by von Engel and Steenbeck is based on the behavior of this region as matrix sheath where ion density n_i is approximately uniform and $n_i >> n_e$. The electric field distribution is linear related to this behavior as

$$\frac{dE}{dx} = en_i = constant \quad \Rightarrow \quad E(x) = E_C(1 - \frac{x}{d}) \qquad 0 < x < d \tag{1.28}$$

where E_C is the field strength at the cathode surface and d is the thickness of the cathode layer. Using Townsend breakdown condition for the cathode layer, provided by $E(x) \backsimeq 0$ for $x > d$, gives us a relation between sheath thickness and E_C,

$$\int \alpha\,(E(x))\,dx = ln\left(1 + \frac{1}{\gamma}\right), \tag{1.29}$$

where

$$\alpha(E) = Ap\,exp\left(-\frac{Bp}{E_C(1 - x/d)}\right). \tag{1.30}$$

Using the relation between field and voltage difference

$$V_C = -\int_0^d E(x)dx \quad \Rightarrow \quad V_C = \frac{E_C d}{2} \tag{1.31}$$

Integration of equation (1.29), which is breakdown condition for cathode layer, results in a equation as

$$\frac{AB(pd)^2}{2V_C} I\left(\frac{2V_C}{Bpd}\right) = ln\left(1 + \frac{1}{\gamma}\right), \tag{1.32}$$

where I is an tabulated integral [1, 2].

A qualitative description of cathode layer based on light emission intensity can be made starting from the cathode surface. Electrons that are emitted from cathode have no sufficient energy for excitation, $\backsim 1eV$, so Aston dark space is formed. After being accelerated to an sufficient energy for excitation the cathode glow appears as the next. Cathode glow can have internal layers that is different in colors based on excitation to different atomic levels ordered from low to higher ones. When the energy of electrons increase above the excitation maximum, the cross-sections decrease and this cause the further decrease in excitation events so cathode dark space is formed. Most of the ionization events and avalanche of electrons occur in this layer, so a large positive space charge is formed here due to non-accelerated heavy ions [1].

1.4.2 Negative Glow and Faraday Dark Space

These two layers is the transition region between cathode layer and positive column as a whole. Avalanche multiplication of electrons along with the end of cathode layer causes a large electron flux. Electrons dissipate some of their energy via collisions related to low level of field strength and the order of energy returns excitation maximum again along with the cathode dark space. Under these conditions the number of excitation events increase

and negative glow appears. Contrary to cathode glow, the order of excited energy levels is inverted from higher to lower ones because electron energy decreases along with the negative glow layer. The electric field strength is decreased to very low levels that electrons lose almost all of their energy along this layer, so before positive column Faraday dark space is formed. Along Faraday dark layer, electric field gradually increases to a value that characterizes the positive column and electrons are re-accelerated in this weak field [1, 11].

1.4.3 Positive Column

This layer is considered as weakly ionized non-equilibrium plasma in which quasineutrality is developed, where this results in an almost constant electrical potential profile. Electrons have random velocity distribution, Druyvesteyn like, that is shifted a little related to the drift towards anode. and have a mean energy on the order of $1 - 2\,eV$. Existence of energetic electrons provides light emission from this column by excitation process but density of light emission is lower than of the negative glow layer. The balance in this region is based on relation between medium variables such as ionization degree, charged particle densities and electric field strength. The loss of charge carriers is determined by ambipolar diffusion to the side walls rather than bulk recombination. This loss is compensated by a weak ionization that needs electron energy on the order of $1 - 2\,eV$. This energy is provided by a weak constant electric field that results in a weak potential difference in this region [1, 11].

1.4.4 Anode Layer

Ion escape from anode and electron drift toward anode result in a negative space charge in this region. Electric field is higher compared to the positive column so that electrons gain energy along this region but before accessing a sufficient energy for excitation, firstly a dark space is developed that is named as anode dark space. Anode glow appears when the excitation event number is increased by the accelerated electrons. The potential fall along anode layer is smaller than in cathode layer and has no effective result in overall character of discharge [2].

1.5 Voltage-Current Curve

The voltage-current curve of a dc glow discharge reflects some important characteristics of these types of discharges. The curve is based on measuring voltage-current values of a discharge gap connected to a circuit that include a resistor R and dc power supply V_{out}. The current is controlled by changing R or V_{out} to maintain target current value. The equation for the potential difference of electrodes is

$$V_a = V_{out} - IR, \tag{1.33}$$

which is plotted in Fig. 1.8 as a load line. The intersection of this line and current axis at $I = V_{out}/R$ shows the limiting maximum value for the current on the circuit. Discharge is formed at the current value corresponding to the intersection of this load line and the curve.

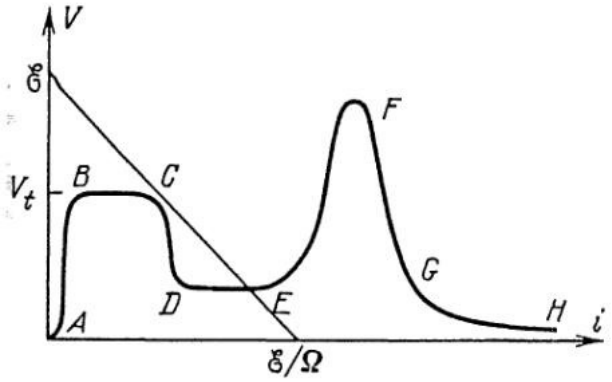

Figure 1.8: Load line with current-voltage curve for glow discharge [1].

For a more deep interpretation the curve is divided into regions between points that are labeled by capital letters, each has a name corresponding to the subtypes of glow discharges. The region A-B corresponds to the non-self-sustained discharge before breakdown which we have mentioned in section 1.3.1. As the current is increased, transition to the self-sustaining discharge region occurs at breakdown voltage V_b. The region B-C corresponds to the well known Townsend dark discharge where voltage is equal to the breakdown value along this region. The current is very weak on the order of $10^{-10} \backsim 10^{-5}\,A$, that corresponds to a low ionization degree. The intensity of light emission is not at considerable levels. The external electric field is not affected by low densities of charged particles and the low space charge so that the potential distribution is almost linear, $E \backsimeq V_b/d$. Although an increasing current requires a more effective ionization process via a stronger field, the constancy of voltage difference along this region indicates an additional contribution to the ionization process that is

known as secondary electron emission from a cold cathode.

If the current is increased further, voltage difference falls lower values throughout the region C-D that has a negative slope characteristic, $dV/dI < 0$, and corresponds to subnormal glow discharge. This region is a transition from dark to glow discharge. The voltage is still higher than in subsequent region. When the current reaches a certain value, the voltage ceases to drop, stays almost constant through the D-E region that is called as normal glow discharge. The voltage continues to stay constant up to a value of order $10^{-1}\,A$. The wideness of this flat line strongly depends on pressure, which increases for higher pressures. A notable behavior of this region is the constant current density at the cathode. As the current is increased, cathode spot reflects this change by expanding on cathode surface holding current density constant. This phenomena was tried to be explained by von Engel and Steenbeck via minimum power principle for the cathode layer but absence of relations to the fundamental laws of physics for this principle is accepted as a big obvious problem in this explanation. In the region for normal glow discharge effective distortion of electric field and potential distribution begin to occur, such as concentrating potential drop between electrodes close to the cathode. When the expansion of cathode spot covers all of cathode surface, subsequent increase in current forces the current density increase on the cathode surface. Voltage begin to increase parallel to this change that refers to entering in a region, E-F, named as abnormal glow discharge. This continues up to the current values on the order of $1\,A$. This level corresponds to heating of cathode by the current that causes a thermal emission of electrons from cathode surface intensively. Further increase in current corresponds to a transition to the arc discharge, F-G, which voltage value decreases to very low levels [1].

1.6 Basic Modelling Approaches: Classification

The modelling of discharges is basicly defined as determination of equations of motion that they obey internally. Actually discharge phenomena is consist of many particles that can be treated as a many particle system. By defining space and velocity coordinates for each of them dependent on time, a set of equations can be constructed to solve numerically. Of course this approach models a discharge truly but solving these equations of motion is an impossible task due to large number of particles even in the case of most powerful computers are used. The thing to do is to approach to this phenomena from a macroscopic point of view such as

defining distribution functions for each type of particle (electrons, ions, neutrals) or consider them as fluids obeying hydrodynamic laws. Main modelling efforts in this area are following on this way by solving these macroscopic equations via simulations on computers.

1.6.1 Kinetic Approach

This approach is based on defining distribution functions for each particle type that provides us all variable mean characteristics of particles via moments such as particle density, flux or mean energy. These distributions are symbolized as $f(\mathbf{r}, \mathbf{v}, t)$ where $\mathbf{r}$, $\mathbf{v}$ and t are independent coordinates for position, velocity and time. Variation of these distribution functions is expressed by the Boltzmann equation,

$$\frac{\partial f}{\partial t} + \mathbf{v} \cdot \nabla f + \mathbf{a} \cdot \nabla_v f = S_C, \tag{1.34}$$

$$\mathbf{a} = \frac{\mathbf{E} + \mathbf{v} \times \mathbf{B}}{m} \tag{1.35}$$

where $\mathbf{a}$ is mean acceleration of the particles, ∇_v refers to the velocity gradient and S_C is source term related to the elastic and inelastic collisions. This equation is coupled with self-consistent electromagnetic fields via acceleration term determined by Maxwell equations. In most modelling efforts energy distribution is used instead of velocity distribution and some approximations such as the two-term expansion to decrease the complexity. However it is difficult to solve this equations if the processor of the computer is not very powerful because even in a one dimensional simulation there are many degrees of freedom, which corresponds to product of equation and element numbers in the discretization process for a numerical calculation [11].

1.6.2 Fluid Approach

Description of each plasma species as fluids decrease the the level of accuracy but results in a less complex system of equations. This approach is based on hydrodynamic fluid equations that are actually continuity equations for plasma species coupling with Maxwell equations via self-consistent fields again. Most basic form is 1-fluid approach which accepts the single species as a fluid and known as MHD approach. Increase in number of types accepted as fluids such as electrons and ions in 2-fluid approach provides more accurate results than for

low number of fluids accepted. The equations can be written in the absence of magnetic field as [11]

$$\frac{\partial n_p}{\partial t} + \nabla \cdot \mathbf{\Gamma}_p = S_p, \tag{1.36}$$

$$\nabla \cdot \mathbf{E} = \frac{\rho}{\varepsilon_0}, \tag{1.37}$$

where p is particle type, $\mathbf{\Gamma}_p$ is the the flux of the particle expressed as the sum of drift and diffusional flux, S_C is source term that expresses the creation or loss of the particles, $\mathbf{E}$ is electric field and ρ is the charge density. These continuity equations are obtained by velocity moments of Boltzmann equation. The determination of transport coefficients such as mobility, diffusion or averaged collision frequencies is a matter of concern in this approach such that this process is dependent on the acceptance of a specific type of distribution but distribution can change in time and space. This problem is solved by relating these coefficients to local electrical field strength in a pure fluid approach but the existence of nonlocal effects significantly decreases the accuracy level of this approach.

1.6.3 Hybrid Modelling Approach

Basically this approach is the combination of kinetic and fluid models. Some types of particles such as heavy ions or neutrals have Maxwellian energy distribution in most discharges so these can be treated as fluids. On the other hand distributions for electrons can differ from a Maxwellian significantly, that results in considerable effects on discharge characteristics where a kinetic approach is a necessity. The degree of hybridity is related to the ratio of usage of these two approaches. For example modelling only fast electrons kinetically decrease the portion of kinetic approach. Most of the researchers carry out their simulations using hybrid approach nowadays.

CHAPTER 2

EXTENDED FLUID MODEL OF A DC GLOW DISCHARGE IN ARGON GAS

2.1 Aims and Motivation

Although a pure fluid approach describe most of the characteristics of discharge phenomena, it does not provide some important information about discharges such as profiles for plasma parameters accurately. Simulations with this approach have been made by many researchers under different conditions as in [15, 18]. Locality feature of this approach does not reflect the discharge behavior in various cases that in fact some nonlocal effects characterize the plasma. This situation forces us to to take care of these nonlocal effects via a hybrid approach or using an extended fluid model. In this case, the approach is based on taking care of these nonlocal effects by adding an energy equation for electron (EEE) additional to the set of continuity equations for plasma species. In this way, the electron transport and collision rate coefficients are related to the mean energy (or temperature) of electrons that is calculated from energy equation. These transport coefficients and reaction rate coefficients for electrons are tabulated in the form of look-up tables that is constructed by Boltzmann solver for electron energy distribution function for an interval of mean electron energy. A third continuity equation for metastable atoms, that can have considerable effects on discharge behavior which is investigated as in various sources [16, 17], is placed additional to the electrons and ions. Lastly, the contribution of surface charges to the regulation of electric field on the dielectric side walls is simulated by an equation in this study. All of these equations are coupled with the Poisson equation via electric field.

These equations are solved in COMSOL Multiphysics software that uses finite element method

for numerical calculations and details can be found from its manuals [28]. All equations are constructed in the general form except for surface charges which is used a weak form for that and they are solved in a cylindrical tube filled with argon gas that has a radius $R = 1.5\,cm$ and gap length $L = 1\,cm$ under $1\,Torr$ and $3\,Torr$ gas pressures using axial symmetry properties in 1D and 2D cylindrical geometry. The discharge volume is connected to a circuit that has a variable resistor in the interval $0 \backsim 100\,M\Omega$ for controlling the current, a capacitor that takes values between 10^{-15} and $10^{-12}\,F$ due to the effects on the stabilization process of numerical calculations and an outer emf source $V_{out} = 500\,V$ that is described in Fig. 2.1.

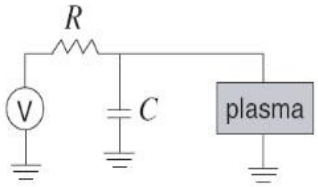

Figure 2.1: Circuit used in the simulations.

This circuit scheme provides us an anode potential for calculations dependent on time and coincides with the load line equation (1.33) for the steady state,

$$\frac{dV_a}{dt} = -\frac{1}{C}\left(I_a - \frac{V_{out} - V_a}{R}\right). \tag{2.1}$$

Here V_{out} is outer emf source, R is resistance, C is capacitance and V_a and I_a are the voltage drop and total current.

2.2 Two-fluid Plasma Model: Derivation of the Model Equations

The fluid equations can be derived from velocity moments of the kinetic equation that includes all of information related to one type of particle. The k^{th} moment is expressed as

$$M_k(\mathbf{r}, t) = \int \mathbf{v}^k f(\mathbf{r}, \mathbf{v}, t) d\mathbf{v} \tag{2.2}$$

integrating over whole velocity space where $d\mathbf{v}$ is infinitesimal volume of that space. These moments which are called as zeroth ($k = 0$), first ($k = 1$) and etc. order, correspond to some macroscopic and average quantities that provide a description for that particle. Especially the first three corresponds to well-known quantities as

$$n(\mathbf{r},t) = \int f(\mathbf{r},\mathbf{v},t)d\mathbf{v} \quad \rightarrow \quad \text{particle density} \tag{2.3}$$

$$\mathbf{\Gamma}(\mathbf{r},t) = \int \mathbf{v} f(\mathbf{r},\mathbf{v},t)d\mathbf{v} = n\mathbf{u} \quad \rightarrow \quad \text{particle flux} \tag{2.4}$$

$$\varepsilon(\mathbf{r},t) = \int \left(\frac{1}{2}\frac{mv^2}{e}\right) f(\mathbf{r},\mathbf{v},t)d\mathbf{v} = \frac{3}{2}nT \quad \rightarrow \quad \text{energy density} \tag{2.5}$$

where $\mathbf{u}$ is the mean fluid velocity, T is the temperature of particle in eV units, m is particle mass and e is electron charge. Using these definitions in the integration process of Boltzmann equation (1.34) provides us the moments of this equation as the conservation laws for the plasma species. The zeroth moment of Boltzmann equation corresponds to conservation law for particle density,

$$\frac{\partial n}{\partial t} + \nabla \cdot \mathbf{\Gamma} = S_C, \tag{2.6}$$

where $\mathbf{\Gamma}$ denotes the particle flux and S_C is collisional source term that describes creation and loss of particles. If the Boltzmann equation is integrated by multiplying with $m\mathbf{v}$, which is first moment of the equation, it corresponds to momentum conservation law,

$$mn\left[\frac{\partial \mathbf{u}}{\partial t} + (\mathbf{u}\cdot\nabla)\mathbf{u}\right] = \mathbf{F}_{ext} + \mathbf{F}_{col}, \tag{2.7}$$

where $\mathbf{F}_{ext}$ and $\mathbf{F}_{col}$ are external and collisional force terms [2, 10].

In our case discharge is modelled by three types of particles, namely, electrons, ions and metastables. The result is three continuity equations for these species. The zeroth and first moments for electrons are expressed as,

$$\frac{\partial n_e}{\partial t} + \nabla \cdot \mathbf{\Gamma}_e = S_e, \tag{2.8}$$

$$m_e n_e\left[\frac{\partial \mathbf{u}_e}{\partial t} + (\mathbf{u}_e\cdot\nabla)\mathbf{u}_e\right] = \mathbf{F}_{ext} + \mathbf{F}_{col}, \tag{2.9}$$

where source terms for particles S_c and momentum source $\mathbf{F}_{ext} + \mathbf{F}_{col}$ is expressed as sum of creation and annihilation terms for particles and external and collisional force terms for momentum. The source term for electron density can be written as

$$S_e = \sum_{k,l=0}^{3} \pm k_{kl} n_k n_l \tag{2.10}$$

where k, l interprets the particle types that contribute to the creation or annihilation of electrons in their collisions and k_{kl} is the their reaction rate constant. The sign of each separate term depends on its contribution type, positive if electrons are created and negative if they annihilated [10, 13]. Source term for momentum conservation can be written as,

$$\mathbf{F}_{ext} + \mathbf{F}_{col} = -en_e\mathbf{E} - \nabla p_e - \tau_e - \sum_{j=0}^{3} m_e n_e \nu_{ej}(\mathbf{u}_e - \mathbf{u}_j), \tag{2.11}$$

where the first term on the right is the force applied by the field, the second is the force due to pressure gradient, the third is the effect of viscosity component which can be ignored in the condition of isotropic pressure and the summation term is the resistive force applied as a result of collisions with other particles [10, 18]. The term ν_{ej} is the collision frequency of electrons with the j-type particle that is expressed in equation (1.13) in terms of reaction rate coefficients. The fluid equations for other species (ions, metastables) can be written in the same format. For ions

$$\frac{\partial n_i}{\partial t} + \nabla \cdot \mathbf{\Gamma}_i = \sum_{k,l=0}^{3} \pm k_{kl} n_k n_l, \tag{2.12}$$

$$m_i n_i \left[\frac{\partial \mathbf{u}_i}{\partial t} + (\mathbf{u}_i \cdot \nabla)\mathbf{u}_i \right] = en_i\mathbf{E} - \nabla p_i - \tau_i - \sum_{j=0}^{3} m_i n_i \nu_{ij}(\mathbf{u}_i - \mathbf{u}_j), \tag{2.13}$$

and for neutral metastables

$$\frac{\partial n_m}{\partial t} + \nabla \cdot \mathbf{\Gamma}_m = \sum_{k,l=0}^{3} \pm k_{kl} n_k n_l, \tag{2.14}$$

$$m_m n_m \left[\frac{\partial \mathbf{u}_m}{\partial t} + (\mathbf{u}_m \cdot \nabla)\mathbf{u}_m \right] = -\nabla p_m - \tau_m - \sum_{j=0}^{3} m_m n_m \nu_{mj}(\mathbf{u}_m - \mathbf{u}_j), \tag{2.15}$$

The key point here is expressing the particle fluxes by using momentum conservation equations via some approximation. For the left-hand side of the electron momentum equation, the time derivative vanishes for a steady state flow and convective derivative of velocity could be ignorable in most cases [10]. For the right-hand side with the help of approximations

$$m_e << m_i, m_m, m_g, \tag{2.16}$$

$$\mathbf{u}_e >> \mathbf{u}_i, \mathbf{u}_m, \mathbf{u}_g, \tag{2.17}$$

and using $p_e = n_e T_e$ for pressure results in an equation

$$n_e \mathbf{u}_e = -\frac{eT_e}{m_e \nu_e} \nabla n_e - \frac{e}{m_e \nu_e} n_e \mathbf{E}. \tag{2.18}$$

Defining flux, diffusion and mobility transport coefficients as

$$\mathbf{\Gamma}_e = n_e \mathbf{u}_e, \qquad D_e = \frac{eT_e}{m_e \nu_e}, \qquad \mu_e = \frac{e}{m_e \nu_e}, \tag{2.19}$$

provides us a more compact form of electron flux,

$$\mathbf{\Gamma}_e = -D_e \nabla n_e - \mu_e n_e \mathbf{E}, \tag{2.20}$$

where T_e is the electron temperature in eV and ν_e is the total collision frequency for electrons [18]. Similar approximations for ions and neutral metastable atoms result in similar expressions for their fluxes. For ions,

$$\mathbf{\Gamma}_i = -D_i \nabla n_i + \mu_i n_i \mathbf{E}, \qquad D_i = \frac{eT_i}{m_i \nu_i}, \qquad \mu_i = \frac{e}{m_i \nu_i}, \tag{2.21}$$

and for neutral metastable atoms

$$\mathbf{\Gamma}_m = -D_m \nabla n_m, \qquad D_m = \frac{eT_m}{m_m \nu_m}, \tag{2.22}$$

where diffusion and mobility coefficients for electrons and ions are related with each other by the Einstein relation as [1]

$$\frac{D_{e,i}}{\mu_{e,i}} = T_{e,i}. \tag{2.23}$$

2.3 Electron Energy Equation

The second moment can be obtained by multiplying the Boltzmann equation with $\frac{1}{2}\frac{mv^2}{e}$, that results in a conservation law for the energy density in the form

$$\frac{\partial \varepsilon}{\partial t} + \nabla \cdot \mathbf{\Gamma}_\varepsilon = S_\varepsilon, \tag{2.24}$$

where ε is chaotic energy density. The energy of drift motion is not included due to its small contribution to the total energy, $u_e << \bar{v}$, where u_e is drift velocity and $\bar{v}$ is mean thermal velocity. For the electrons,

$$\varepsilon = \frac{3}{2} n_e T_e. \tag{2.25}$$

The flux term includes conductional and convectional transport of this energy and defined as

$$\mathbf{\Gamma}_\varepsilon = -\kappa \nabla T_e + \frac{5}{2} n_e T_e \mathbf{u}_e, \tag{2.26}$$

where $\kappa = \frac{5}{2} n_e D_e$ is the heat conduction coefficient for electrons. Using definition of electron flux term (2.17-19) instead of $n_e \mathbf{u}_e$, we obtain an equation for energy flux as the sum of diffusion and drift terms,

$$\mathbf{\Gamma}_\varepsilon = -\frac{5}{3} D_e \nabla \varepsilon - \frac{5}{3} \mu_e \varepsilon \mathbf{E}. \tag{2.27}$$

The source term can be divided into three groups as Joule heat sourced by electric field, energy loss by elastic collisions and by inelastic collisions. Joule heat and elastic loss term is defined as

$$J_{heat} = -e \mathbf{\Gamma}_e \cdot \mathbf{E}, \tag{2.28}$$

$$S_{el} = -\frac{3}{2} \left(\frac{m}{M} \right) n_e \nu_{el} (T_e - T_g), \tag{2.29}$$

where m is electron mass, M is argon atom mass, ν_{el} is elastic energy loss frequency and T_g is gas temperature. For the the inelastic loss term, different inelastic collisional reactions were taken into account that contribute to source term for electron energy as negative or positive,

$$S_{inel} = \sum_{k,l=0}^{3} \pm k_{kl} n_k n_l U_{kl}, \tag{2.30}$$

where U_{kl} is the electron energy lost or gain in one type of collision between k-type and l-type particle [13, 21, 25, 26] .

2.4 Plasma Transport Coefficients

In a pure fluid approach transport coefficients such as mobility and diffusion are calculated by local field approximation (LFA) dependent on electric field strength or considered as constants but this approach provides poor results for discharge characteristics in the case of high electric field strength, for instance at cathode layer. For most of the heavy particles (ions, neutrals) this is not a problem generally but for light particles such as electrons it leads to inaccurate results. More realistic approach relates these electron transport coefficients to its mean energy (or temperature) to take care into some nonlocal effects. The most common way of relating these coefficients to mean energy is two-term approximation for distribution function that provides relations to temperature for the coefficients.

For the electrons drifting in a medium, the distribution function can be divided into two terms as isotropic and anisotropic part. Defining the anisotropy axis overlapping with the direction of electric field, it can be expressed as

$$f \backsimeq f_0 + \frac{v_z}{v} f_1 = f_0 + f_1 \cos\theta \qquad\qquad \mathbf{E} = E_z \hat{\mathbf{z}} \tag{2.31}$$

in spherical coordinates and if $f_1 << f_0$. Using this expression in the Boltzmann equation and integrating it by multiplying $\cos\phi$ and $\sin\phi\cos\phi$ separately, results in two equations for f_0 and f_1,

$$\frac{\partial f_0}{\partial t} + \frac{v}{3}\frac{\partial f_1}{\partial z} - \frac{e}{3mv^2} E_z \frac{\partial (v^2 f_1)}{\partial v} = C, \tag{2.32}$$

$$\frac{\partial f_1}{\partial t} + v\frac{\partial f_0}{\partial z} - \frac{e}{m} E_z \frac{\partial f_0}{\partial v} = -\nu_m(v) f_1, \tag{2.33}$$

where C is collisional contribution as a source term to the spatial and temporal changes in distribution function and $\nu_m(v)$ is the effective momentum transfer frequency. The net flux of electrons can be found by using approximated expression for distribution function (2.31) in the flux equation (2.4) [2],

$$\mathbf{\Gamma} = \int \mathbf{v}(f_0 + f_1 \cos\theta) d\mathbf{v} = \left[\frac{4\pi}{3}\int_0^\infty v^3 f_1 dv\right]\hat{\mathbf{z}}. \tag{2.34}$$

For a steady state distribution, the expression taken from equation (2.32) for f_1 and using this in the flux expression (2.34) after some approximation results in an equation for the flux of electrons,

$$\mathbf{\Gamma}_e = -D_e \frac{dn_z}{dz} - \mu_e n_e E_z, \tag{2.35}$$

where D_e and μ_e are diffusion and mobility coefficients that are related to the symmetric part of distribution function with the expressions [2],

$$D_e = \frac{4\pi}{3n_e} \int_0^\infty \frac{v^4}{\nu_m(v)} f_0 \, dv, \tag{2.36}$$

$$\mu_e = -\frac{4\pi e}{3mn_e} \int_0^\infty \frac{v^3}{\nu_m(v)} \frac{df_0(v)}{dv} dv. \tag{2.37}$$

For these coefficients we only need the knowledge of isotropic part of distribution function and cross-section data for collisions. The equations (2.32) and (2.33) for f_0 and f_1 are difficult to solve analytically unless sufficient approximations is made such as considering the plasma collisionless. Due to this reason researchers try to solve these equations numerically by Boltzmann solvers improved as packages (CFD-ACE, Bolsig, Bolsig+). In these solvers, energy is used as a coordinate instead of velocity via transformation,

$$d\varepsilon = \frac{m}{e} v \, dv, \tag{2.38}$$

with cross-section data tables for each plasma interaction. The above equations for f_0 and f_1 transform into energy dependent equations as

$$\frac{\partial f_0}{\partial t} + \frac{\bar{\gamma}}{3} \varepsilon^{1/2} \frac{\partial f_1}{\partial z} - \frac{\bar{\gamma}}{3} \varepsilon^{-1/2} \frac{\partial (\varepsilon E f_1)}{\partial \varepsilon} = C, \tag{2.39}$$

$$\frac{\partial f_1}{\partial t} + \bar{\gamma} \varepsilon^{1/2} \frac{\partial f_0}{\partial z} - E \bar{\gamma} \varepsilon^{1/2} \frac{\partial f_0}{\partial \varepsilon} = -n_g \sigma_m \bar{\gamma} \varepsilon^{1/2} f_1, \tag{2.40}$$

where $\bar{\gamma} = (\frac{2e}{m})^{1/2}$, E is electric field, n_g is gas particle density and σ_m is momentum transfer cross-section. Using some approximation such as transferring temporal and spatial dependence of distribution function into the electron density, $f(\varepsilon, z, t) \backsimeq F(\varepsilon) n(z, t)$, results in a drift-diffusion type equation for the energy dependent isotropic part. Mobility and diffusion coefficients are expressed as dependent on this isotropic part similar to equations (2.36) and (2.37) as

$$\mu_e = -\frac{\bar{\gamma}}{3n_g} \int_0^\infty \frac{\varepsilon}{\tilde{\sigma}_m} \frac{\partial F_0}{\partial \varepsilon} \, d\varepsilon, \qquad\qquad D_e = \frac{\bar{\gamma}}{3n_g} \int_0^\infty \frac{\varepsilon}{\tilde{\sigma}_m} F_0 \, d\varepsilon, \tag{2.41}$$

where F_0 is the only energy dependent isotropic distribution and $\tilde{\sigma}_m$ is the effective momentum transfer cross-section. The details of these calculations can be found in many sources related to solutions of Boltzmann equation such as in [2, 24, 25].

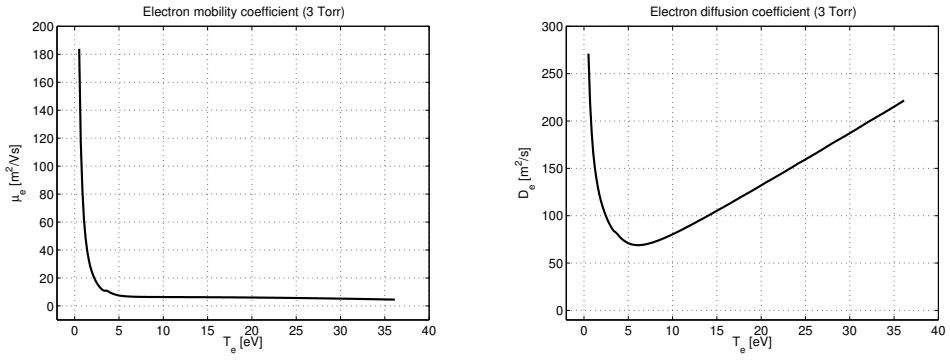

Figure 2.2: Mobility, μ_e, and diffusion, D_e, coefficients for electrons in 3 $Torr$ pressure argon gas.

The essential goal of this process is finding a solution for isotropic part, f_0, of the distribution function. All other quantities are related to this part somehow. Transport coefficients in argon gas that we calculated from a local Boltzmann equation dependent on energy are plotted in Fig. 2.2 for electrons. We use these data as look up tables in our study, applying interpolation and extrapolation.

The coefficients for ions and metastable atoms are defined in various sources [1, 23]. Ions mobility coefficient in argon gas is taken as

$$\mu_i = \left(\frac{0.25}{p}\right) \frac{m^2}{V \cdot s \cdot Torr}, \tag{2.42}$$

where p is pressure in $Torr$. Diffusion coefficient for ions is calculated by Einstein relation

$$D_i = \mu_i \, T_i, \tag{2.43}$$

where T_i is expressed dependent on the electric field strength in its own gas [1],

$$T_i = T_g + \frac{1}{6} \frac{M}{e} \mu_i^2 \, E^2. \tag{2.44}$$

The diffusion coefficient for metastable atoms is taken as

$$D_m = \frac{1.08 \times 10^{-2}}{p} \, \frac{m^2}{s \cdot Torr}. \tag{2.45}$$

2.5 Plasma-chemical Reactions Taken Into Account

There are many collisional process that should be taken into account for more accurate results. These collisional processes including mainly elastic collisions, direct and stepwise ionization, Penning ionization, excitation and deexcitation of metastable atoms for argon gas, can be

expressed by chemical reaction symbolization . The reactions that we use in our study is tabulated below with their threshold energies and rate constants [2, 20, 25].

Table 2.1: Collisional reactions that are taken into account in the study [20, 25].

Symbol	Type	Reaction	$\Delta E(eV)$	Coefficient
R_1	Elastic collision	$e + Ar \longrightarrow e + Ar$	$\backsim 0$	Boltz.
R_2	Direct ionization	$e + Ar \longrightarrow Ar^+ + 2e$	-15.8	Boltz.
R_3	Excitation1	$e + Ar \longrightarrow Ar^*(4s) + e$	-11.4	Boltz.
R_{3b}	De-excitation	$e + Ar^* \longrightarrow Ar + e$	+11.4	Boltz.
R_4	Excitation2	$e + Ar \longrightarrow Ar(4p) + e$	-13.1	Boltz.
R_5	Stepwise ionization	$e + Ar^* \longrightarrow Ar^+ + 2e$	-4.4	Boltz.
R_6	Penning ionization	$Ar^* + Ar^* \longrightarrow Ar + Ar^+ + e$	+7.0	$6.2 \times 10^{-16} m^3/s$
R_7	Radiation	$Ar^* \longrightarrow Ar + \hbar w$	–	$1.0 \times 10^7 s^{-1}$

2.6 Reaction Rates

Reaction rate coefficients derived from the isotropic part of the distribution function as

$$k = \int_0^\infty \sigma(\varepsilon)\sqrt{\varepsilon} f_0(\varepsilon) d\varepsilon \tag{2.46}$$

and obtained from the solution of a local Boltzmann equation in the form of look-up tables dependent on energy for a usable energy range [20, 24, 25, 27]. These are used in the source terms for electron continuity and energy equations related to the defined reaction types that contribute to the creation or annihilation of electrons or electron energy . The reaction rates for Maxwellian metastable atoms are calculated by using Arrhenius's law in Table. 2.1. The calculated reaction rates for electrons are plotted in Fig. 2.3 and used by applying interpolation and extrapolation in our simulation.

2.7 Governing Equations

The governing equations that contribute to the formation of discharge include Poisson equation for electric field, three continuity equations for electrons, ions and metastable atoms, electron energy equation (EEE) and surface charge equation on side walls. Surface charge

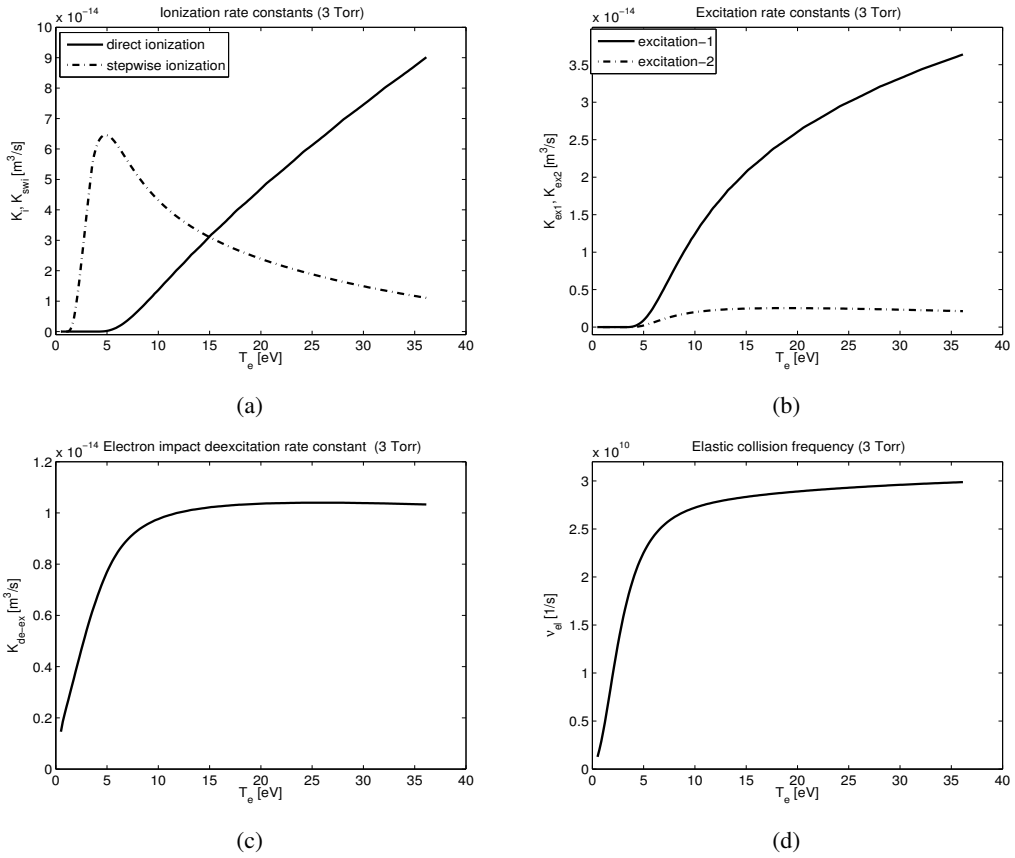

(a) (b) (c) (d)

Figure 2.3: Reaction rate coefficients for (a) direct (K_i) and stepwise (K_{swi}) ionization, (b) excitation-1 (K_{ex1}) and excitation-2 (K_{ex2}), (c) electron impact deexcitation (K_{de-ex}) and (d) elastic collision frequency (ν_{el}) in 3 $Torr$ argon gas tabulated in Table 2.1

is simulated as accumulation of charges on walls dependent on the difference in the directed fluxes of electrons and ions. All of these equations are presented below.

Poisson equation,

$$\nabla \cdot \mathbf{E} = \frac{\rho}{\varepsilon_0} \qquad \mathbf{E} = -\nabla\Phi \qquad \rho = e(n_i - n_e). \tag{2.47}$$

Continuity equations,

$$\frac{\partial n_e}{\partial t} + \nabla \cdot (-D_e \nabla n_e - \mu_e n_e \mathbf{E}) = R_2 + R_5 + R_6, \tag{2.48}$$

$$\frac{\partial n_i}{\partial t} + \nabla \cdot (-D_i \nabla n_i + \mu_i n_i \mathbf{E}) = R_2 + R_5 + R_6, \tag{2.49}$$

$$\frac{\partial n_m}{\partial t} + \nabla \cdot (-D_m \nabla n_m) = R_3 - R_{3b} - R_5 - 2R_6 - R_7, \tag{2.50}$$

where $R_i = K_i n_{e,m} n_{g,m}$ is related to reactions in the Table 2.1.

Electron energy equation,

$$\frac{\partial \varepsilon}{\partial t} + \nabla \cdot \left(-\frac{5}{3} D_e \nabla \varepsilon - \frac{5}{3} \mu_e \varepsilon \mathbf{E} \right) = S_\varepsilon, \tag{2.51}$$

$$S_\varepsilon = J_{heat} + S_{el} + \sum_{i=2}^{7} R_i \Delta E_i, \tag{2.52}$$

where R.H.S is according with equations (2.28-2.30).

Surface charge equation,

$$\frac{d\sigma_s}{dt} = e \left(\Gamma_{di} - \Gamma_{de} \right), \tag{2.53}$$

where Γ_{di} and Γ_{de} are the directed fluxes for ions and electron onto the side walls. These fluxes are defined by using thermal motion additional to the drift motion towards the walls in the form [21, 22, 23],

$$\Gamma_{dp} = \frac{1}{4} n_p v_p + \mathbf{a_p} \mu_p n_p E_n, \tag{2.54}$$

where p defines the particle type, $v_p = \sqrt{\frac{8eT_p}{\pi m}}$, and E_n is the normal component of electric field at the wall. The coefficients a_p are expressed as

$$a_p = \begin{cases} 1 & sgn(q)\hat{\mathbf{n}} \cdot \mathbf{E} \geq 0, \\ 0 & sgn(q)\hat{\mathbf{n}} \cdot \mathbf{E} < 0. \end{cases} \tag{2.55}$$

For electrons drift motion towards the walls is ignored due to smallness with respect to thermal electron motion, $a_e = 0$. For neutral metastable atoms it automatically takes the value, $a_m = 0$, and for ions it can take the values $a_i = 0, 1$.

2.8 Geometry and Boundary Conditions

The discharge geometry is the cylindrical tube that have a radius $R = 1.5\,cm$ and gap length $L = 1\,cm$. The equations are solved for 1D and 2D dimensions using the axial symmetry in the cylindrical coordinates as shown in Fig. 2.4. The equations are solved for the cross-section of the cylindrical tube and expanded to whole volume by using the axial symmetry property of the geometry. For 1D calculations, these equations are solved only on the symmetry axis, so that no surface charge equation is needed.

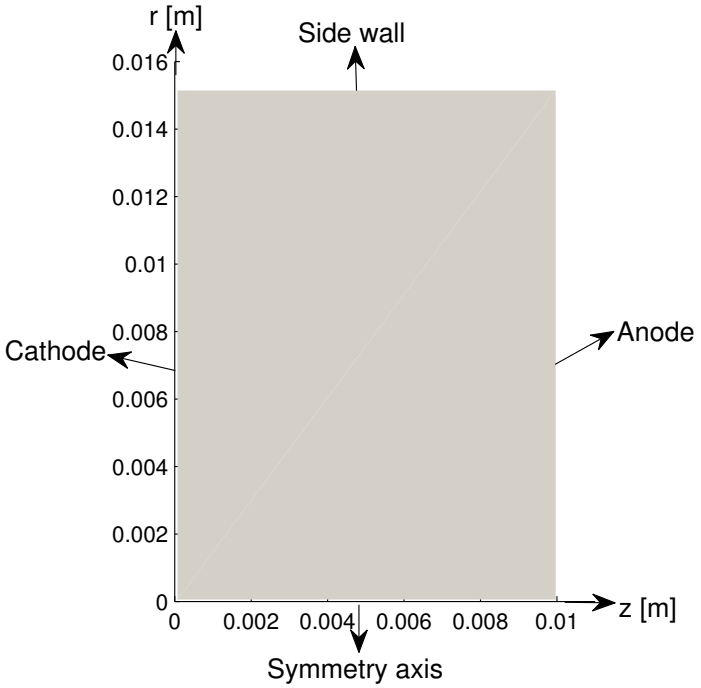

Figure 2.4: Computational domain used in the study.

The boundary conditions for continuity equations are defined by the Neumann type where the flux values are defined on the boundaries. For 1D simulations these are expressed only on cathode and anode. For 2D simulations, additionally the conditions on the side walls of the volume are involved. The fluxes on boundaries are related to directed motion of particles onto the walls.

At the cathode,

$$\text{ions} \qquad \hat{\mathbf{n}} \cdot \mathbf{\Gamma}_i = \Gamma_{id} \tag{2.56}$$

$$\text{electrons} \qquad \hat{\mathbf{n}} \cdot \mathbf{\Gamma}_e = \frac{1}{4} n_e v_e - \gamma \Gamma_{id} \tag{2.57}$$

$$\text{metastables} \qquad \hat{\mathbf{n}} \cdot \mathbf{\Gamma}_m = \frac{1}{4} n_m v_m \tag{2.58}$$

$$\text{electron energy} \qquad \hat{\mathbf{n}} \cdot \mathbf{\Gamma}_\varepsilon = \frac{5}{12} v_e \varepsilon - 2 T_e \gamma \Gamma_{id} \tag{2.59}$$

$$\text{Potential} \qquad \Phi = 0 \tag{2.60}$$

At the anode,

$$\text{ions} \qquad \hat{\mathbf{n}} \cdot \mathbf{\Gamma}_i = \Gamma_{id} \tag{2.61}$$

$$\text{electrons} \qquad \hat{\mathbf{n}} \cdot \boldsymbol{\Gamma}_e = \frac{1}{4} n_e v_e \tag{2.62}$$

$$\text{metastables} \qquad \hat{\mathbf{n}} \cdot \boldsymbol{\Gamma}_m = \frac{1}{4} n_m v_m \tag{2.63}$$

$$\text{electron energy} \qquad \hat{\mathbf{n}} \cdot \boldsymbol{\Gamma}_\varepsilon = \frac{5}{12} v_e \varepsilon \tag{2.64}$$

$$\text{Potential} \qquad \Phi = V_a \qquad \text{(Eq. 2.1)} \tag{2.65}$$

At the side walls,

$$\text{ions} \qquad \hat{\mathbf{n}} \cdot \boldsymbol{\Gamma}_i = \Gamma_{id} \tag{2.66}$$

$$\text{electrons} \qquad \hat{\mathbf{n}} \cdot \boldsymbol{\Gamma}_e = \frac{1}{4} n_e v_e \tag{2.67}$$

$$\text{metastables} \qquad \hat{\mathbf{n}} \cdot \boldsymbol{\Gamma}_m = \frac{1}{4} n_m v_m \tag{2.68}$$

$$\text{electron energy} \qquad \hat{\mathbf{n}} \cdot \boldsymbol{\Gamma}_\varepsilon = \frac{5}{12} v_e \varepsilon \tag{2.69}$$

$$\text{Potential} \qquad \hat{\mathbf{n}} \cdot \mathbf{E} = -\frac{e\sigma_s}{\varepsilon_0} \tag{2.70}$$

At the symmetry axis,

$$\text{ions} \qquad \hat{\mathbf{n}} \cdot \boldsymbol{\Gamma}_i = 0 \tag{2.71}$$

$$\text{electrons} \qquad \hat{\mathbf{n}} \cdot \boldsymbol{\Gamma}_e = 0 \tag{2.72}$$

$$\text{metastables} \qquad \hat{\mathbf{n}} \cdot \boldsymbol{\Gamma}_m = 0 \tag{2.73}$$

$$\text{electron energy} \qquad \hat{\mathbf{n}} \cdot \boldsymbol{\Gamma}_\varepsilon = 0 \tag{2.74}$$

$$\text{Potential} \qquad \hat{\mathbf{n}} \cdot \mathbf{E} = 0 \tag{2.75}$$

CHAPTER 3

NUMERICAL RESULTS

3.1 Numerical Approach

The numerical simulations are carried out by COMSOL Multiphysics package program which are used by many researchers for calculations due to its effectiveness. It is a well prepared programming package that allows researchers construct a simulation model easily via its user friendly interface. Except for the surface charge equation, the equations were modelled by the general form due to convenience for convergence of the calculations. For the surface charge equation, the weak form is used to simulate charge accumulation on the dielectric side walls. The discretization in the solution volume is based on the finite element method (FEM) that is described in package manuals. Time-dependent solution process is governed by implicit backward differential formulas (BDF) that the solutions for each time step is tested by a stabilization process for a limited error defined numerically. The meshes for 1D and 2D simulations are in quadrilateral form which are constructed more thinner for the higher gradient regions of variables (eg., potential) compared with the other regions.

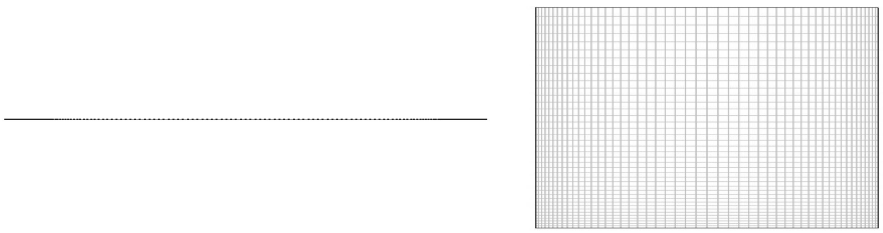

(a) (b)

Figure 3.1: 1D and 2D meshes used in the study.

3.2 Current-Voltage Characteristics

The results for current-voltage characteristics (CVC) under the pressures $1\,Torr$ and $3\,Torr$ in 1D and 2D geometries are plotted in Fig. 3.2 in comparison with each other. For 2D solutions the breakdown voltage is slightly higher than in 1D solutions due to the charge loss in the side walls, which results in a lower ionization degree that must be compensated with a stronger electric field. Throughout the CVCs, the three modes of glow discharges are

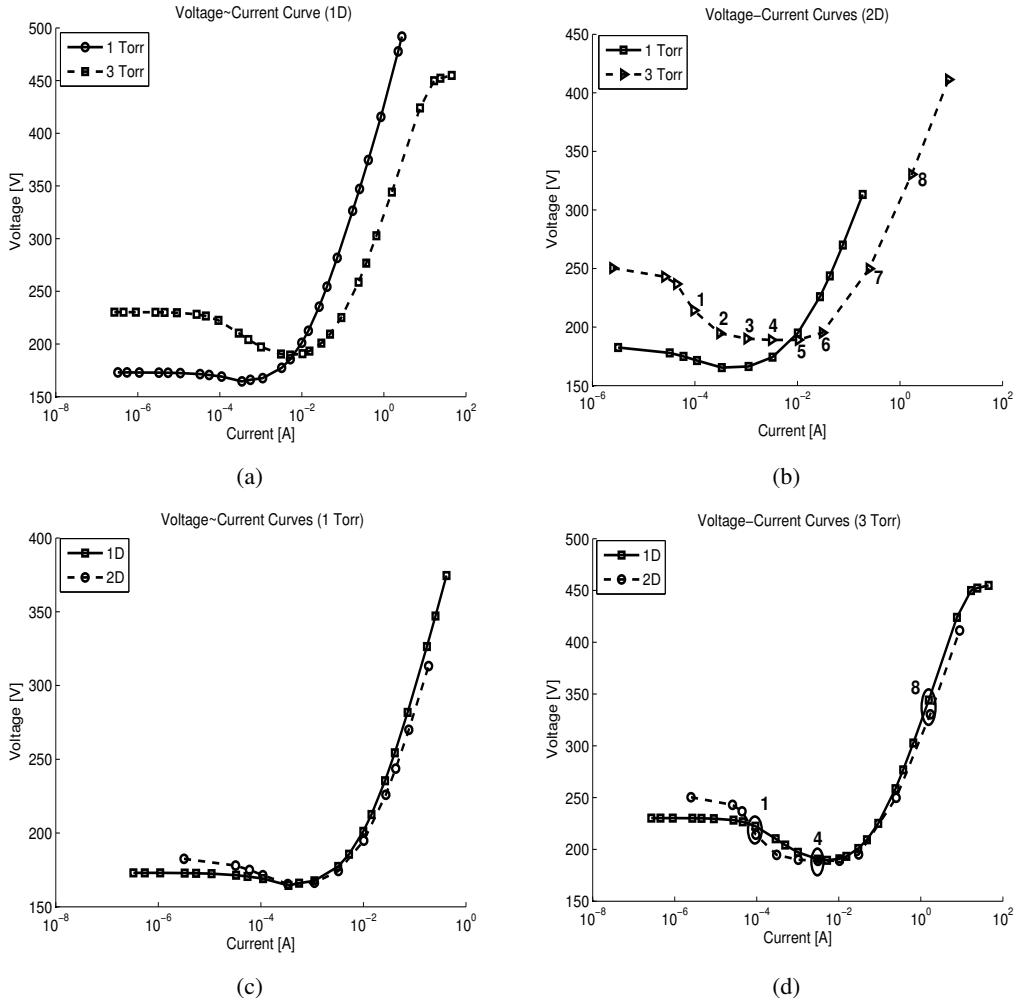

Figure 3.2: Voltage-current curves for 1D and 2D simulations for argon gas, $p = 1\,Torr$ and $3\,Torr$, $R = 1.5\,cm$, $L = 1\,cm$. The points are numbered for comparison of axial profiles of plasma parameters in 1D and 2D for subnormal, normal and abnormal regimes.

distinguishable, namely, subnormal (1-3), normal (3-5) and abnormal (5-8) regimes. These regions are characterized by the the points 1, 4, 8 with the currents $I_1 = 9.3\,\mu A$, $I_4 = 3.1\,mA$, $I_8 = 1.6\,A$ for the pressure, $p = 3\,Torr$ (Fig 3.2-b). The width of CVC at the normal glow region increases in 2D solution that reflects the cathode spot behavior. For higher pressure

value the breakdown voltage increase again which shows that this pressure region corresponds to the right side of minimum voltage throughout the Paschen curve for argon gas (Fig. 1.4). The width of normal glow region increases again for the higher pressure.

3.3 Comparison of Axial Profiles

The axial profiles for discharge parameters are plotted for the three modes of glow discharges, namely, for the subnormal, normal and abnormal modes. In Fig. 3.3 and Fig. 3.4, the density profiles of electrons and ions are shown in the logarithmic scale.

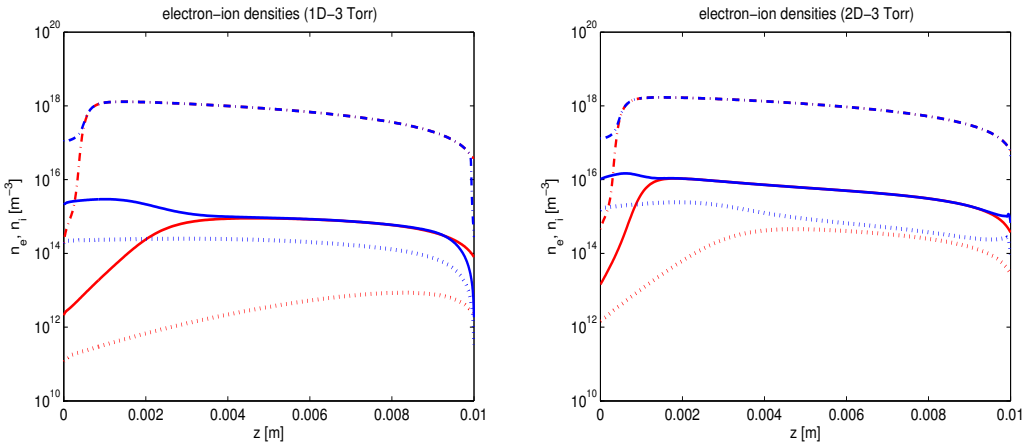

(a) (b)

Figure 3.3: Electron (red) and ion (blue) density axial profiles in logarithmic scale, (a) 1D and (b) 2D for subnormal (dotted lines,1), normal (solid lines,4) and abnormal (dash-dot lines,8) regimes in argon discharge, $p = 3\,Torr$. The numbers in parentheses indicate the points in Fig. 3.2-d. The currents corresponding to these points are $I_1 = 9.3\,\mu A$, $I_4 = 3.1\,mA$, $I_8 = 1.6\,A$.

Throughout the subnormal to abnormal regimes the densities for electrons and ions increase which reflects the ionization degree. The formation and expansion of a quasineutral region in between the electrodes are recognizable in the Fig. 3.3. The cathode fall behavior develops in this process clearly (Fig 3.4-a). Comparing 1D and 2D axial profiles of plasma parameters shows that the results resemble in abnormal regime more commonly. A noticeable difference in 1D and 2D calculations is the electric field behavior at anode layer where it is reversed in 2D simulations (Fig. 3.4-b).

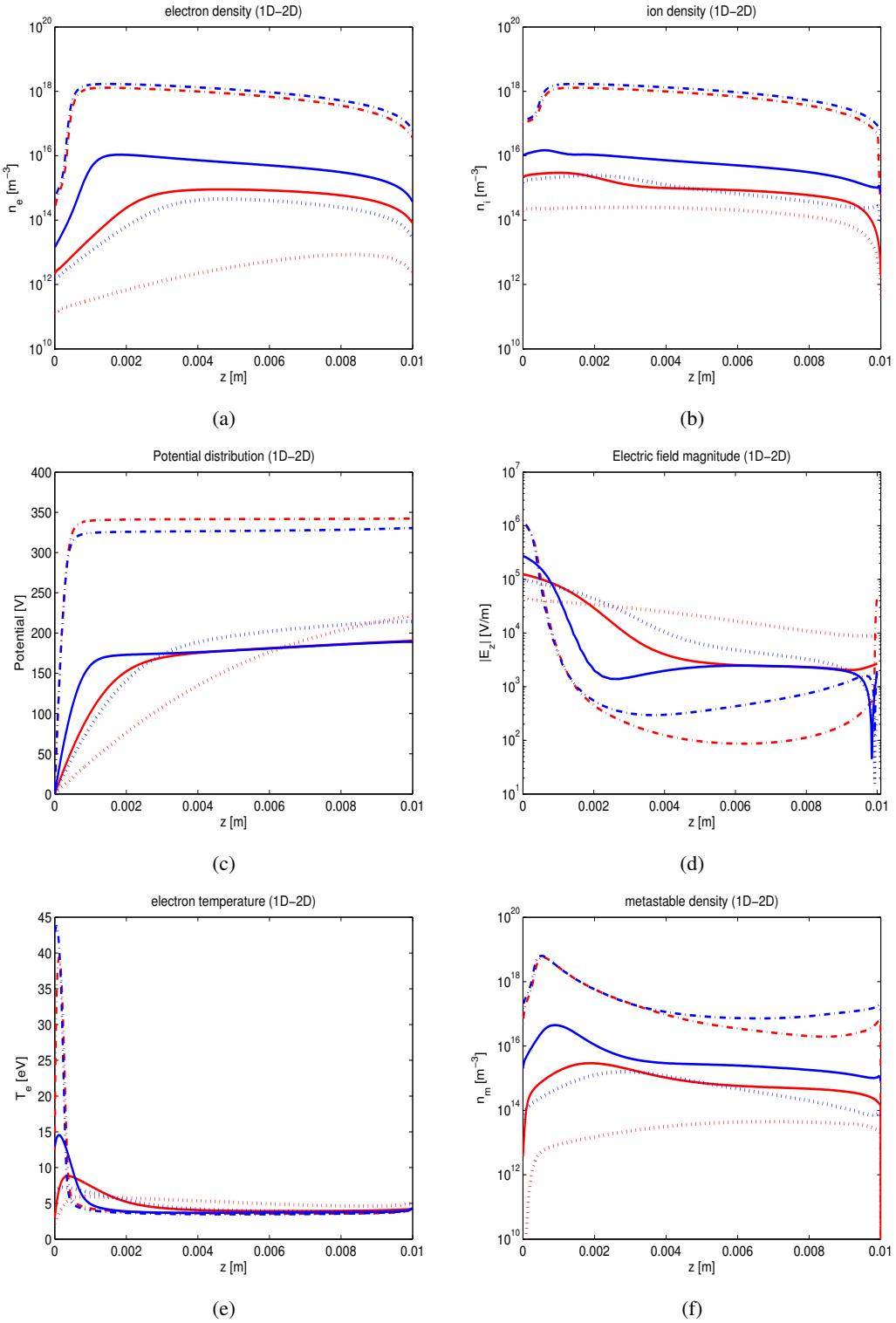

Figure 3.4: Comparison of 1D (red) and 2D (blue) calculations for axial electron density (a), ion density (b), potential (c), electric field magnitude (d), electron temperature (e), metastable density (f) profiles for subnormal (dotted lines, 1), normal (solid lines, 4) and abnormal (dash-dot lines, 8) regimes in argon discharge, $p = 3\,Torr$. The numbers in parentheses indicate the points in Fig. 3.2-d. The currents corresponding to these points are $I_1 = 9.3\,\mu A$, $I_4 = 3.1\,mA$, $I_8 = 1.6\,A$.

3.4 2D Profiles

Results of 2D calculations show that profiles for plasma parameters are strongly dependent on the boundary condition on the dielectric side walls. The loss of charged particles and metastables and charge accumulation on the side walls results in a rearrangement of the profiles when compared with the 1D results.

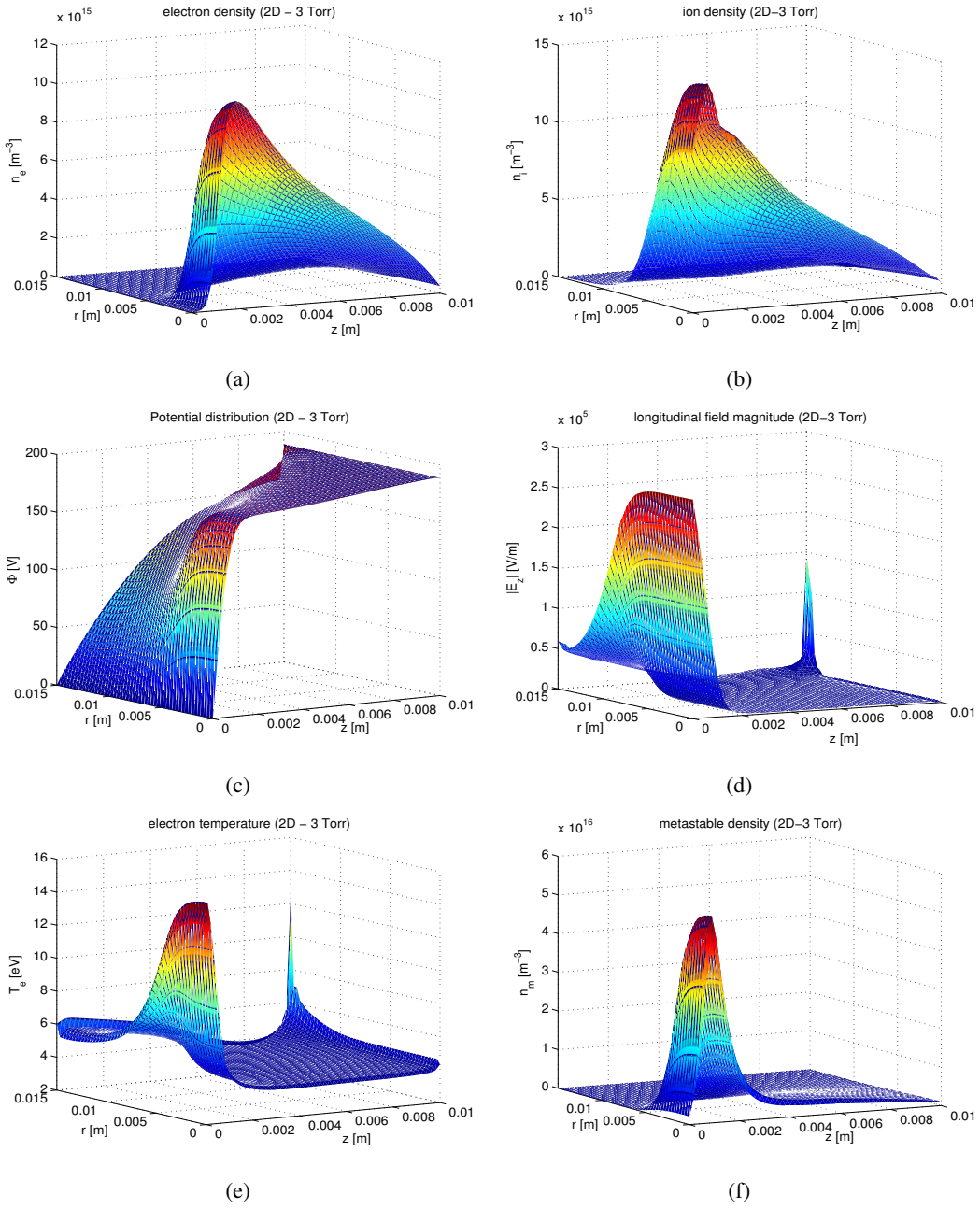

Figure 3.5: 2D plasma parameter profiles for $p = 3\,Torr$ argon gas, $I = 3.1\,mA$ corresponding to the point 4 labeled in Fig. 3.2-b, $R = 1.5\,cm$ and $L = 1\,cm$.

Throughout the subnormal to abnormal regions the plasma is expanded in the radial direction. The higher values for density profiles, potential drop and electron temperature close to the central symmetry axis near the cathode reflects the cathode spot formation in this region. The 2D profiles of discharge plasma parameters ($n_e, n_i, n_m, T_e, \Phi, |E_z|$), corresponding to the normal glow regime (point 4 in Fig. 3.2-b) at $p = 3\,Torr$, are presented in Fig. 3.5.

3.5 Radial Profiles

Radial profiles of cathode current densities corresponding to subnormal, normal and abnormal modes and a detailed behavior throughout the normal regime are presented in Fig. 3.6 for 2D calculations. The profiles around V_{min}, which corresponds the point 4 in Fig. 3.2-b, reflects the constancy of current density on cathode spot that expands itself until all the cathode surface is covered. The solid lines in the Fig. 3.6-b corresponding the points 3, 4, 5 in the Fig. 3.2-b reflects the formation and the width of cathode spot on cathode surface. The flat regions on these lines correspond the central section that most of the current flow in.

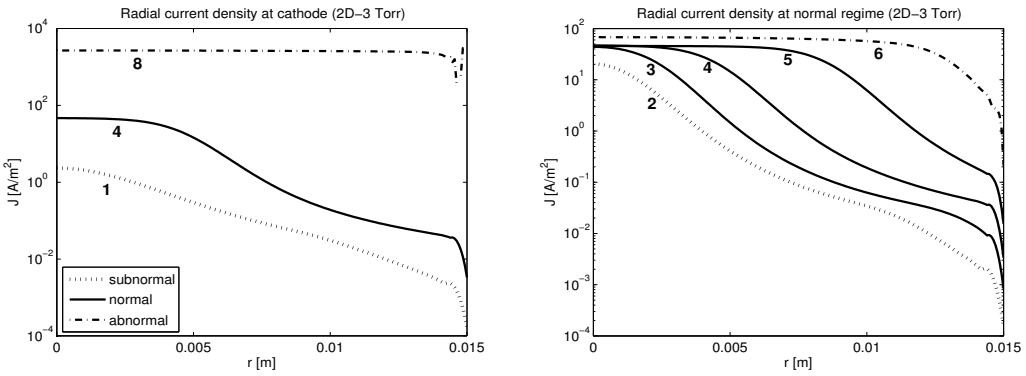

(a) (b)

Figure 3.6: Radial current density profiles on cathode surface in logarithmic scale for $p = 3\,Torr$. The numbers indicate the points in Fig. 3.2-b and the corresponding currents for these points are $I_1 = 9.3\,\mu A$, $I_2 = 0.3\,mA$, $I_3 = 1.0\,mA$, $I_4 = 3.1\,mA$, $I_5 = 10.4\,mA$, $I_6 = 30.5\,mA$, $I_8 = 1.6\,A$.

3.6 Comparison With Different Numerical Data

The simulation results in our study is in agreement with the published data by Arslanbekov et al. The differences in results are related to usage of different boundary conditions that can have considerable effects on the profiles for plasma parameters. A comparison of 1D calculations for $3\,Torr$ pressure argon gas for the current-voltage curves and profiles of electron and ion density, potential and electron temperature is presented in Fig. 3.7.

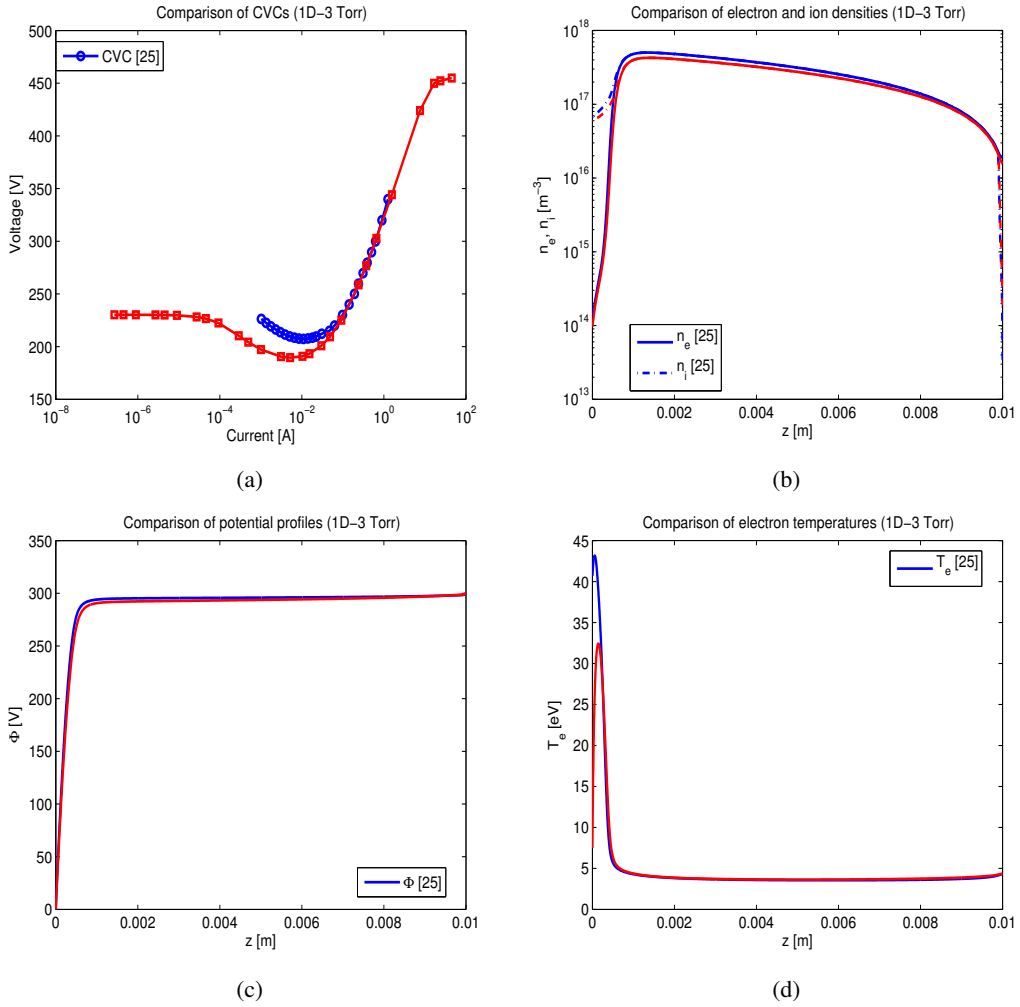

Figure 3.7: Comparison of our results (red) with the data in [25] (blue) for 1D calculations where $p = 3\,Torr$ and potential drop between the electrodes, $V_a = 300\,V$. (a) Current-voltage curves, (b) electron and ion density profiles, (c) potential profiles and (d) electron temperature

.

CHAPTER 4

CONCLUSION

We have simulated the glow discharge in argon gas for the pressures $1\,Torr$ and $3\,Torr$ in 1D and 2D geometry using an extended fluid approach that includes electron energy equation in addition to the continuity equations for plasma species. The electron transport coefficients and electron-impact reaction rate coefficients are related to the electron temperature rather than electric field, where temperature is calculated from the electron energy equation. These coefficients are produced by Boltzmann solver in the form of look-up tables dependent on mean electron energy and used in calculations applying interpolation and extrapolation. Additionally, the effect of metastable atoms and surface charge accumulation on the dielectric side walls are taken into consideration by appropriate equations.

Presented numerical results show the well-known properties of glow discharges such as voltage-current characteristics as well as density, potential and electron temperature profiles. Breakdown voltage for argon gas in the considered pressure regime is on the order of $200 \backsim 250\,V$ is in agreement with the data presented in the literature [1]. The regimes known as Townsend dark regime, subnormal, normal and abnormal regimes in the CVCs are clearly distinguishable.

Simulations demonstrated development of the sheath formations near the electrodes and side walls. The density values on the order of $10^{14} \backsim 10^{17}\,m^{-3}$ correspond to the expected values that are presented by different authors for weakly ionized gases and show the expected increasing behavior between Townsend and abnormal regimes. The formation of voltage drop close to cathode is caused by the accumulation of a positive space charge near the cathode.

In general, structure of glow discharges consists a cathode layer by a noticeable potential drop on the order of several hundred volts and where quasineutrality violated , a quasineutral

region with a low electric field strength and low electron temperature on the order of $4\,eV$ and anode layer with a weak potential drop or sheath formation near it. The distribution of discharge parameters shows a noticeable change in 2D solutions due to surface charge accumulation on the side walls. The loss of charged particles at dielectric side walls rearrange the distribution of discharge parameters in the discharge volume, which leads to increase in values for breakdown voltage, electric field and densities.

The characteristic behavior of cathode spot such as holding the current density constant for the applied voltage near the minimum of CVC is presented in Fig. 3.6 that corresponds to the normal glow region. Finally, the instabilities occurred for electric field and electron temperature at the intersection of dielectric side walls and anode in 2D calculations (Fig. 3.5-d and Fig. 3.5-e) are related to the definition of surface charge accumulation on the side walls. The equation for this boundary process is expressed in the most basic form due to absence of accurate reflection and sticking coefficient data in the literature for the charged particles arriving to the side walls.

REFERENCES

[1] Raizer Y. P.; Gas Discharge Physics, p. 1-378, Berlin: Springer-Verlag (1991)

[2] Lieberman M. A., Lichtenberg A. J.; Principles of Plasma Discharges and Materials Processing, p. 14-80, New Jersey: John Wiley & Sons (2005).

[3] Goldston R. J., Rutherford P. H.; Introduction to Plasma Physics, p. 85-180, Bristol:IOP (1995).

[4] Llewellyn-Jones F.; The Glow Discharge and an Introduction to Plasma Physics, p. 1-23, New York: John Wiley & Sons (1966).

[5] Friedman A., Kennedy L.; Plasma Physics and Engineering, p. 204-505, New York:Taylor and Francis (2004).

[6] Boyd T. J. M., Sanderson J. J.; The Physics of Plasmas, p. 48-76, New York: Cambridge University (2003).

[7] Marcus R. K., Broekaert J. A. C.; Glow Discharge Plasmas in Analytical Spectroscopy, p.157, West Sussex: John Wiley & Sons (2003).

[8] Chen F. F.; Introduction to Plasma Physics and Controlled Fusion, p. 53-285, New York:Plenum (1974).

[9] Bellan P. M.; Fundamentals of Plasma Physics, p.1-69, New York Cambridge University (2006)

[10] Rozhansky V. M., Tsendin L. D.; Transport Phenomena In Partially Ionized Plasma, p. 1-75, London and New York: Taylor & Francis (2001)

[11] Piel A.; Plasma Physics, p. 107-130, London and New York: Springer (2010)

[12] Gurnett Donald A., Bhattacharjee A; Introduction To Plasma Physics With Space and Laboratory Applications, p. 5-18, 137-166. New York: Cambridge University (2005)

[13] Miyomato K.; Plasma Physics and Controlled Nuclear Fusion, p. 1-78, Springer-Verlag Berlin Heidelberg (2005)

[14] R.D. Hazeltine, and F.L.; The Framework of Plasma Physics, p. 1-46, Waelbroeck: Westview Boulder CO. (2004).

[15] Rafatov I. R., Akbar D., Bilikmen S.; Phys. Lett. A, 367, 114-119 (2007)

[16] Lymberopoulos Dimitris P. and Economouâ Demetre J.; J. Appl. Phys. 73 (8), 3668 (1993)

[17] Bogaerts A. and Gijbels R.; Phys. Rev. A 52 (5), 3743 (1995)

[18] Surzhikov Sergey T., Shang Joseph S.; Journal of Computational Physics 199, 437-464 (2004)

[19] Arslanbekov Robert R., Kolobov Vladimir I.; J. Phys.D:Appl. Phys. 36, 2986-2994 (2003)

[20] Farouk T., Bakhtier F. Staack D., Gutsol A., Fridman A.; Plasma Sources Sci. Technol. 15, 676-688 (2006)

[21] Sakiyama Y., Graves D.B., Stoffels E.; J. Phys. D.: Appl. Phys. 41, 095204 (9pp) (2008)

[22] Donko Z., Hartman P., Kutasi K.; Plasma Sources Sci. Technol. 15, 175-186 (2006)

[23] Fiala A., Pitchford L.C., Boeuf J.P.; Phys. Rev. E 49 (6), 5067 (1994)

[24] Hagelaar G.J.M., Pitchford L.C.; Plasma Sources Sci. Technol. 14, 722-733 (2005)

[25] Arslanbekov R, Kolobov V.; J. Phys. D: Appl. Phys. 36, 64089 (2003)

[26] G. J. M. Hagelaar, F. J. de Hoog, and G. M. W. Kroesen,; Phys. Rev. E 62 (1), 1452-1454 (2000).

[27] V.I. Kolobov; Computational Materials Science 28, 302-320 (2003)

[28] Comsol Multiphysics^{TM} 3.4, COMSOL Inc., http://www.comsol.com (2011)